## PAPER

Check for updates

# Investigating the anticancer potential of 4-phenylthiazole derived Ru(II) and Os(II) metalacycles†

Paul Getreuer, [ID] [a,b] Laura Marretta, [ID] [c] Emine Toyoglu,[a] Orsolya Dömötör, [ID] [d] Michaela Hejl,[a] Alexander Prado-Roller, [ID] [a] Klaudia Cseh,[a] Anton A. Legin, [ID] [a] Michael A. Jakupec, [ID] [a,e] Giampaolo Barone, [ID] [c] Alessio Terenzi, [ID] [c] Bernhard K. Keppler [ID] [a,e] and Wolfgang Kandioller [ID] *[a,e]

In this contribution we report the synthesis, characterization and *in vitro* anticancer activity of novel cyclo-metalated 4-phenylthiazole-derived ruthenium(II) (**2a–e**) and osmium(II) (**3a–e**) complexes. Formation and sufficient purity of the complexes were unambigiously confirmed by $^{1}$H-, $^{13}$C- and 2D-NMR techniques, X-ray diffractometry, HRMS and elemental analysis. The binding preferences of these cyclometalates to selected amino acids and to DNA models including G-quadruplex structures were analyzed. Additionally, their stability and behaviour in aqueous solutions was determined by UV-Vis spectroscopy. Their cellular accumulation, their ability of inducing apoptosis, as well as their interference in the cell cycle were studied in SW480 colon cancer cells. The anticancer potencies were investigated in three human cancer cell lines and revealed IC$_{50}$ values in the low micromolar range, in contrast to the biologically inactive ligands.

## Introduction

Since the landmark discovery of cisplatin,[1] platinum-based anticancer agents have been effectively utilized for the treatment of numerous cancer types on a global scale.[2,3] However, dose-dependent side effects, such as nephrotoxicity, neurotoxicity, hepatotoxicity, and resistances severely hamper their efficacy.[4] This implies a strong need for novel metal-based drugs, which more selectively target tumor cells and overcome resistance problems, while featuring unique mechanisms of action.[5,6]

Within the class of metallodrugs, ruthenium-based compounds have garnered attention as promising alternative anticancer agents. Notably, ruthenium(III) complexes, specifically sodium *trans*-[tetrachlorido-bis(1*H*-indazole) ruthenate(III)] (BOLD-100, Fig. 1) and imidazolium *trans*-[Ru(*N*-imidazole)(*S*-DMSO)Cl$_4$] (NAMI-A), have shown effective inhibition of tumor metastasis and angiogenesis. BOLD-100, the sodium analog of indazolium *trans*-[tetrachlorido-bis(1*H*-indazole)ruthenate(III)] (KP1019, Fig. 1), features enhanced aqueous solubility com-

[a]*Institute of Inorganic Chemistry, Faculty of Chemistry, University of Vienna, Waehringer Straße 42, 1090 Vienna, Austria.*
*E-mail: wolfgang.kandioller@univie.ac.at*
[b]*Vienna Doctoral School in Chemistry (DoSChem), Faculty of Chemistry, University of Vienna, Waehringer Straße 42, 1090 Vienna, Austria*
[c]*STEBICEF-Department, University of Palermo, Viale delle Scienze, Ed. 17, 90128 Palermo, Italy*
[d]*Department of Molecular and Analytical Chemistry, University of Szeged, Dóm tér 7-8, 6720 Szeged, Hungary*
[e]*Research Cluster "Translational Cancer Therapy Research", University of Vienna, Waehringer Straße 42, 1090 Vienna, Austria*

†Electronic supplementary information (ESI) available: Ligand synthesis, $^{1}$H and $^{13}$C NMR spectra, mass spectra, X-ray diffraction analysis, stability in aqueous solution, MTT-data, G-quadruplex interaction studies, amino acid interaction data, apoptosis and cell cycle investigations. CCDC 2296745–2296747, 2296749–2296751 and 2296753. For ESI and crystallographic data in CIF or other electronic format see DOI: https://doi.org/10.1039/d4dt00245h
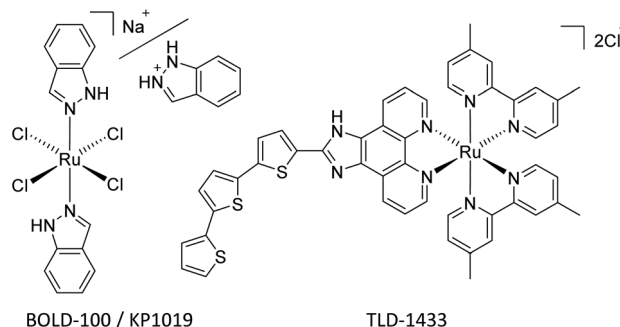


Fig. 1 Investigational Ru-based anticancer drugs BOLD 100 (Na$^+$)/ KP1019 (indazolium) and TLD1433.

pared to its indazolium counterpart. Successful clinical phase I trials were conducted, making BOLD-100 the second ruthenium-based anticancer drug to move on to a phase II trial. Throughout phase I trials, it has already demonstrated therapeutic activity in solid tumors, such as non-small cell lung cancer, colorectal carcinoma and particularly in gastrointestinal neuroendocrine tumors.[7–9] Furthermore, recent reports of an ongoing phase IIa trial showed promising results.[10]

Activation by reduction of the Ru(III) center to the more reactive Ru(II) species is assumed to be an essential step in the mechanism of action.[11] Hence, Ru(II) compounds moved to the spotlight of ruthenium-based anticancer research. TLD-1433 (or [Ru(4,4′-dmb)₂(IP-3T)](Cl)₂ [where: 4,4′-dmb = 4,4′-dimethyl-2,2′-bipyridine; IP = imidazo[4,5-$f$]-[1,10]phenanthroline; 3T = α-terthiophene], Fig. 1) is currently the furthest developed Ru(II) antitumor drug, undergoing a clinical phase II trial for its potential in photodynamic therapy of nonmuscle-invasive bladder cancer.[12–14]

Stabilization of the Ru(II) center under normal physiological conditions can be achieved by the coordination of π-bonded arenes, which affords the class of highly stable pseudo-octahedral "piano-stool" complexes. These Ru(II)-arene organometallics provide a versatile framework that paves the way for straightforward refinement of antitumor properties through ligand variation.[15–17] Sadler's and Dyson's groups investigated organo-ruthenium complexes extensively, which resulted in the development of the two most prominent and advanced representatives of this substance class, namely, Sadler's RAED organometallics and Dyson's RAPTA complexes.[15,18–21]

Most Ru(II) arene compounds feature a halido leaving group, priming the complex for biological interactions *via* substitution of the halido moiety by a water molecule. This process is presumed to be pivotal in the mechanism of action[22] and emphasized by the activation-by-aquation hypothesis.[23]

Due to limited stability of conventional bidentate motifs (*e.g. O,O*; *N,O*; *S,O*), the application of the respective organometallics as anticancer drug candidates remains severely restricted.[24] Consequently, scientists emphasized alternatives with improved stability under physiological conditions, which led us to the investigation of *C,N*-coordination motifs in bidentate ligands for cytotoxic organometallics.[15,17,25] Over the last years, especially *C,N*-coordinated Ru(II) metalacycles featuring 2-arylthiazole,[26] 2-phenylindole,[27] 2-phenylpyridin,[28] benzimidazole,[29,30] 4-phenyltriazole[15,17] and 2-phenylben-

zothiazole[25] scaffolds have been reported. In contrast, the biological properties and the cytotoxicity of osma(II)cycles of the general form [Os(arene)L_CΛN Cl] remain nearly unexplored and were only investigated by Boff *et al.*,[31] Riedl *et al.*[15] and Mokesch *et al.*[25] In every case, promising cytotoxicities in the low micromolar range were reported.

To extend the library of cyclometalated antitumor agents, the present contribution introduces the very robust and versatile 4-phenylthiazole scaffold. We report on the straightforward synthesis and characterization of Ru(II) and Os(II) arene complexes bearing 4-phenylthiazoles as *C,N*-chelates. We show the cytotoxicity of the synthesized compounds in human lung adenocarcinoma (A549), colon adenocarcinoma (SW480), and ovarian teratocarcinoma (CH1/PA-1) cells. Furthermore, we explore the impact of five 4-phenylthiazole derivatives as *C,N* bidentate ligands and the difference between Ru(II) and Os(II) metal centers on the biological activity. To elucidate the mechanism of action, we also investigated the cellular accumulation, impact on cell cycle distribution and the compounds' potential to induce apoptosis in SW480 cells. In addition to these findings, the complexes' ability to interact with G-quadruplex (G4) structures is also subject of discussion.

## Results and discussion

### Synthesis

Five 4-phenylthiazole ligands were synthesized based on the procedure of Lee *et al.*[32] utilizing a straightforward Suzuki cross-coupling reaction. 4-Bromothiazole was coupled with the appropriate arylboronic acid or ester, using tetrakis(triphenylphosphine)Pd(0) as catalyst and after workup the desired ligands were obtained in moderate to good yields (42%–89%, Scheme 1).

Cyclometalation was achieved *via* sp² C–H bond activation. The dimeric precursor [Ru(*p*-cym)Cl₂]₂ or [Os(*p*-cym)Cl₂]₂ (*p*-cym = *p*-cymene) is thereby converted to M(*p*-cym)(OAc)₂ using an excess of sodium acetate. The activated organometallic species was then converted with the ligand, where in the first step the thiazole nitrogen binds coordinatively to the metal center. A subsequent deprotonation of the *ortho* hydrogen of the phenyl residue by uncoordinated acetate *via* an intramolecular S_E3-mechanism and simultaneous coordination concludes the cyclometalation reaction.[33] Lastly, the acetato-complex [M(*p*-cym)(L_CΛN)(OAc)] undergoes transition
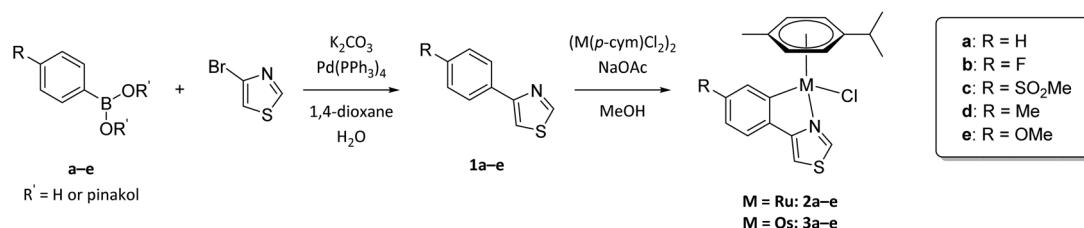


**Scheme 1** Synthesis of substituted 4-phenylthiazole ligands **1a−e** and their Ru(II) (**2a−e**) and Os(II) (**3a−e**) metalacycles.

to the desired chlorido products. However, with high acetate catalyst loadings a fraction of acetato-complex remains in the reaction mixture. To improve the conversion to the chlorido-complexes, a novel step in the work-up of cyclometalation procedures was introduced and exploited. In fact, the dissolution of the crude product in $CH_2Cl_2$ and subsequent vigorous stirring with brine grants sufficient chloride ions to convert residual acetato-derivatives.

While precipitation from $CH_2Cl_2$ solution with *n*-hexane can be utilized to purify the target complexes, column chromatography proves to be much more efficient, affording the desired metalacycles in elemental analysis purity and moderate to good yields (46%–86%).

## Characterization

The synthesized compounds were characterized by means of standard analytical methods such as $^1H$-, $^{13}C$- and 2D-NMR, high-resolution electrospray ionization mass spectrometry (ESI-MS), X-ray crystallography, and elemental analysis.

$^1H$- and $^{13}C$-NMR confirmed the formation of the desired cyclometalates. Prior studies with related triazole organometallics showed that the chlorido leaving group is readily replaced by DMSO and due to similar behavior of the complex series $CDCl_3$ was used as NMR solvent.[15] Metal coordination breaks the symmetry of the substituted phenyl moiety, resulting in various splitting motifs depending on the substituent in position 4 as can be seen in the $^1H$ spectra of the formed complexes (Fig. S1–S15†). Due to the electron withdrawing effect, the $SO_2Me$ residue shifts the protons *para* and *meta* to the metalated carbon to lower fields. Lastly, the proton signals of the 4-fluorophenyl ring were easily assignable due to the presence of additional (H,F) couplings.

Thiazole protons always appeared as two doublets, whereas H-2 was shifted downfield (0.2–0.3 ppm) upon metal coordination, due to the electron withdrawing effect of the metal center. Interestingly, the thiazole H-4 proton is considerably shifted upfield (0.2–0.3 ppm) and found around 7.3–7.5 ppm. Furthermore, the arene protons of *p*-cymene can be observed as four separate doublets in contrast to the free dimeric precursor where the four aromatic cymene protons were found as two doublets. In case of mesyl bearing **2c**, ethyl acetate traces (0.25 eq.) from the purification *via* column chromatography remained in the sample even after drying for several days at 50 °C *in vacuo*.

High-resolution mass spectrometry of the cyclometalates revealed the presence of the chlorido abstracted species [M – Cl]⁺, as well as sodium adducts [M + Na]⁺ in some cases. Additionally, the Os(ɪɪ)-metalacycles were observed as dimeric sodium adducts [2M + Na]⁺ (Fig. S16–S25†).

Single crystals of **2a**, **2b**, **2d** and **2e** as well as **3a**, **3b** and **3d**, suitable for X-ray diffraction analysis, were obtained by slow diffusion of *n*-hexane into DCM or $CHCl_3$ complex solutions. Detailed crystal data, data collection parameters, structure refinement details and CCDC-codes and be inferred from the ESI (Fig. S26–S32 and Tables S1–S8†). As depicted in the crystal structure of **2a** (Fig. 2) the complexes adopt the so-
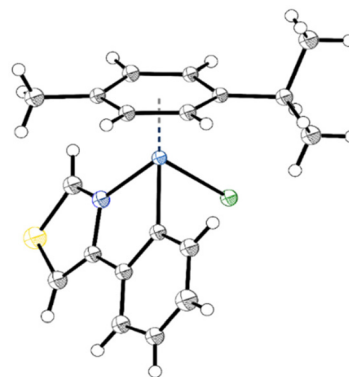


Fig. 2 Crystal structure of ruthenacycle **2a**.

called piano-stool configuration. Therein, the π-bonded *p*-cym represents the seat and the mono- and bidentate ligands the three legs of the stool. The investigated complexes are representatives of the monoclinic space groups $P2_1/n$ (**2a**, **2e**, **3a**, **3b**) or $P2_1/c$ (**2b**, **2d**, **3d**). Both enantiomers were found in the elemental unit of the complexes. Within the pseudo-octahedral configuration of the compounds, a new distorted five-membered ring arises from the chelating ligand and the metal center. Thus, the phenyl and thiazole rings are locked in plane, featuring low torsion angles of 0.4(4)–4.8(3)° along the thiazole-phenyl bond. The coordination bonds exhibit remarkable similarity between the two metal counterparts, as anticipated due to a mere 0.01 Å difference in their atomic radii (Ru: 1.34 Å, Os: 1.35 Å). Os–N (2.079(3)–2.101(7) Å) and Os–C (2.069 (7)–2.081(4) Å) bonds were found to be slightly longer than their Ru analogs (2.065(4)–2.079(2) Å and 2.061(2)–2.070(3) Å, respectively). On the other hand, the osmium metal center is marginally closer to the arene ring (1.6820(2)–1.6847(3) Å) compared to Ru analogs (1.6905(3)–1.6956(3) Å), with ring slippages of 0.062–0.095 Å. A similar trend was observed with the related 4-phenyltriazole based Ru(ɪɪ)- and Os(ɪɪ)-arene compounds by Riedl *et al.*[15] The metal-chlorido bond lengths (2.4124(11)–2.4232(6) Å) are consistent with anticipated values.[15,25,34–36]

## Stability in aqueous solution

The aqueous stability of the metalacyles was determined *via* UV-Vis spectroscopy under pseudo-physiological conditions over 24 h at 20 °C using 1% DMF as solubilizer in PBS (40 μM compound concentration, pH 7.4, Fig. S33–S42†). DMF was used instead of DMSO to avoid the formation of solvent adducts.[15] Based on the obtained spectra, the ruthenium(ɪɪ) and osmium(ɪɪ) compounds undergo (micro)precipitation (except complex **2c**), which results in a slight decrease of absorption over time; however, no new peaks, isosbestic points or shifts of peak maxima were observed over 24 h.

## Chloride ion affinity

The chloride-ion affinity of **2a** and **2c** was investigated *via* UV-Vis spectroscopy at various KCl concentrations at 25 °C

using 1% DMF as solubilizer in water. The hydrolysis of the M–Cl bond was found to be relatively fast, the equilibrium was reached within *ca.* 10 min, therefore batch samples were prepared and the $H_2O/Cl^-$ exchange constants were calculated based on the obtained UV-Vis spectra (Fig. S43 and S44†). The determined constants are $\log K(H_2O/Cl^-) = 1.16 \pm 0.01$ for **2a** and $1.26 \pm 0.01$ for **2c**. Accordingly, the chlorido ligand dissociates in >99% when the complex is dissolved in pure water. In the presence of 100 mM chloride ion concentration (corresponds to the chloride ion level of blood plasm) the original chlorido complexes are present in 60% (**2a**) and 65% (**2c**), which are in very good agreement with the results of $^1H$ NMR experiments (Fig. S45†).

### Antiproliferative activity and cellular accumulation

The ruthenium(II) compounds (**2a–e**), the osmium(II) analogs (**3a–e**), as well as the corresponding ligands (**1a–e**) were evaluated for their antiproliferative activity in human lung adenocarcinoma (A549), colon adenocarcinoma (SW480), and ovarian teratocarcinoma (CH1/PA-1) cell lines by means of the colorimetric MTT assay (Table 1 and Fig. S46, S47†). Unlike the free 4-phenylthiazole ligands, for which $IC_{50}$ values were not reached with the tested concentrations of up to 200 μM, the metalacycles **2a–e** and **3a–e** demonstrated significant cytotoxic effects with $IC_{50}$ values in the low micromolar range. In general, all tested complexes exhibit their highest activity in the broadly chemosensitive CH1/PA-1 cell line and the lowest in the multidrug-resistant A549 cell line. Previously published antiproliferative activity of comparable ruthenium(II) based metalacycles of the general form $[Ru^{II}(arene)L_{C\wedge N}]$ was found in the same range as the investigated 4-phenylthiazole derived ruthenacycles (2-aryldiazole (10–150 μM),[26] 2-phenylindole (0.45–5.4 μM),[27] 2-phenylpyridine (3–100 μM),[28] benzimidazole (1–150 μM),[29,30] 4-phenyl-1,2,3-triazole (0.65–109 μM),[15,17] 2-phenylbenzothiazole (2.7–16 μM)[25]). In contrast to ruthenacycles, osmium analogs $[Os^{II}(arene)L_{C\wedge N}]$ are relatively sparse in literature. Nevertheless, their antiproliferative activity corresponds well with Riedl's 4-phenyl-1,2,3-triazole (0.98–34 μM)[15] and Mokesch's 2-phenylbenzothiazole (1.2–8.7 μM)[25] scaffolds.

Remarkably, they exhibit slightly higher cytotoxicity than the ruthenium counterparts. Within this compound series, mesyl bearing metalacycles **2c** and **3c** show the most potent cytotoxic effect. On the other hand, the methyl analogs, **2d** and **3d**, exhibit the lowest antiproliferative activity within the tested cell lines. The differences between $IC_{50}$ values of the least and most potent representative of each series generally indicate a moderate impact of the variable substituent.

To further elucidate the effects of the varying substituents of the metalacycles, the cellular accumulation of the ruthenium series **2a–e** in SW480 cells was assessed. Additionally, the calculated lipophilicity of the unbound ligand (clog P), which serves as a representative measure for the corresponding complexes, was determined using molinspiration (Table 2). Surprisingly, cellular accumulation is most pronounced for both the least lipophilic mesyl derivative **2c** and the very lipophilic fluoro derivative **2b**. Except for the comparatively low $IC_{50}$ value of **2a**, a clear trend of higher compound cytotoxicities at higher cellular accumulation was found. A direct comparison of $IC_{50}$ values and drug accumulation is illustrated in Fig. S48.†

### Mechanism of action

The rather high cytotoxicity of the metalacycles compelled us to conduct further investigations into the mechanism of action of this compound class.

**DNA binding studies.** Considering that DNA is a major target of many metal-based drug candidates,[37] the synthesized metalacycles were tested for their interaction with DNA oligonucleotides organized either in B-double helix or G-quadruplex secondary structures. Interestingly, Ru-arene complexes have been rarely tested against G4 structures,[38–42] although these DNA motifs are largely involved in cancer development.[43] In detail, DNA binding properties of compounds **2a**, **2c**, and **2d** were investigated by means of fluorescence resonance energy transfer melting assay (FRET), circular dichroism (CD) and mass spectrometry (MS). The compounds were selected with regard to their cytotoxicities to elucidate structure activity relationships. Furthermore, we deepened our study through molecular docking calculations.

Concerning the FRET assay, compounds **2a**, **2c**, and **2d** were incubated at different concentrations with selected oligonucleotides (Tables S9 and S10†) folded as G4s (c-*KIT1* and c-*MYC*) or duplex B-DNA (dsDNA). c-*KIT1* and c-*MYC* were selected considering that these DNA structures form in the

**Table 1** Inhibition of cancer cell growth in three human cancer cell lines, determined by the MTT assay (exposure time: 96 h). 50% Inhibitory concentrations (means ± standard deviations) from at least three independent experiments

| Compound | A549 [μM] | SW480 [μM] | CH1/PA-1 [μM] |
|---|---|---|---|
| **1a–e** | >200 | >200 | >200 |
| **2a** | 24 ± 4 | 9.5 ± 0.7 | 3.0 ± 0.9 |
| **2b** | 16 ± 1 | 8.6 ± 0.9 | 3.4 ± 0.2 |
| **2c** | 12 ± 1 | 5.1 ± 0.4 | 1.6 ± 0.4 |
| **2d** | 34 ± 3 | 19 ± 2 | 14 ± 2 |
| **2e** | 27 ± 1 | 17 ± 1 | 7.3 ± 0.4 |
| **3a** | 17 ± 1 | 9.3 ± 1.1 | 3.0 ± 0.2 |
| **3b** | 10 ± 1 | 7.1 ± 0.3 | 2.0 ± 0.4 |
| **3c** | 10 ± 1 | 4.4 ± 0.5 | 0.83 ± 0.14 |
| **3d** | 17 ± 1 | 9.3 ± 1.6 | 3.7 ± 0.6 |
| **3e** | 14 ± 1 | 7.1 ± 1.2 | 2.2 ± 0.3 |

**Table 2** Cellular accumulation of compounds **2a–e** (50 μM, 0.5% DMF in MEM) in SW480 cancer cells (exposure time: 2 h) and calculated log P (clog P) values of the corresponding free ligands

| Compound | Ru/cell [fg] | clog P (free ligand) |
|---|---|---|
| **2a** | 183 ± 13 | 2.54 |
| **2b** | 326 ± 39 | 2.71 |
| **2c** | 326 ± 14 | 1.41 |
| **2d** | 183 ± 14 | 2.99 |
| **2e** | 263 ± 11 | 2.60 |

promoters of the corresponding oncogenes *c-kit* and *c-myc* and have a key role in regulating their expression.[44] The ability of the cyclometalates to stabilize such structures was quantified by the increase of the oligonucleotides' melting temperatures ($\Delta T_{1/2}$). Interestingly, no discernible stabilization with any of the compounds was observed with dsDNA up to a 1/20 [DNA]/[compound] ratio (Fig. S49†). In contrast, a concentration dependent effect was observed when the metal-based compounds were incubated with the G4 motifs (Fig. S50 and Table S10†). The most effective stabilization profile was achieved with c-*MYC* and compound **2c**, which induced a $\Delta T_{1/2}$ of approximately 15 °C at the 1/20 ratio, reaching 18 °C at 1/30 (Fig. 3a). In contrast, lower $\Delta T_{1/2}$ values for c-*KIT1* were obtained and only at the highest ratios for **2a** and **2d**. In comparison to other metal complexes that induce higher $\Delta T_{1/2}$ values at lower concentration,[45] the tested compounds can be regarded as modest G4 stabilizers. Despite this, they exhibit a promising preference for G4 over B-DNA and show a clear concentration dependent G4 stabilization. No perturbation of the c-*KIT1* and c-*MYC* structures was observed as a consequence of the interaction with the metalacycles. Their circular dichroism signatures, typical of parallel G-quadruplexes (a positive and a negative band centered at 263 and 241 nm, respectively), remain unaltered after titration of the oligos with increasing amounts of **2a**, **2c** and **2d** (Fig. S51†). As a control, titrations were performed using calf thymus DNA (ct-DNA) selected as B-DNA model, and its structure also remained unaffected (Fig. S52†).

As mentioned, the synthesized Ru(II) arene compounds feature a halido leaving group, which after activation-by-aquation, can be substituted by a DNA base. Hence, mass spectrometry was employed to study the adduct formation of **2a**, **2c**, **2d** with 9-ethylguanine. When the cyclometalates (0.2 mM) were incubated with an excess of 9-ethylguanine (0.6 mM) in H$_2$O (4% DMF as solubilizer) for 2 h at room temperature they all readily formed adducts with the selected DNA base model (Fig. S53–S55†). Given such a result and effective stabilization observed in FRET experiments, adduct formation of ruthenacycle **2c** with the oligonucleotide c-*MYC* was also investigated

by MS (Fig. 3b). Peaks corresponding to the five charged mass of c-*MYC* (found: 1397.2403, calcd: 1397.2318) and of the **2c**-c-*MYC* adduct (found: 1491.8361, calcd: 1491.8332) were found (Fig. S56†), confirming a tight interaction between the two entities.

The interaction between the selected G4 structures and compounds **2a**, **2c** and **2d** (*R* and *S* enantiomers) was investigated by molecular docking calculations. The NMR resolved structures of c-*MYC* (PDB id: 1XAV) and c-*KIT1* (PDB id: 2O3M) served as G4 models. The structures of both *R* and *S* enantiomers of **2a**, **2c** and **2d** were optimized by DFT calculations. Out of 50 possible poses, the most representative ones of each cluster are reported in Fig. S57 and S58† for c-*MYC* and c-*KIT1*, respectively.

Overall, the interaction of the metalacycles with the G4 structures takes place within the DNA grooves rather than with the G-tetrads in contrast to what is observed with classic planar G4 binders which interact with the top/end guanine tetrads. Interestingly, the docking free binding energy values (Tables S11 and S12†) suggest that the *R* enantiomers non-covalently interact better with both c-*KIT1* and c-*MYC* G4s, with compound **2c** (*R*) being the most effective c-*MYC* binder, corroborating FRET results (Fig. 3c and Fig. S49, S50†). It is worth mentioning that docking results were obtained using the aqua complexes. The reported poses are driven by electrostatic forces and are the step before substitution of the water molecule by a DNA base.

**Amino acid interaction.** Amino acid interaction studies were conducted to elucidate the behavior and potential binding partners of the synthesized metalacycles within intricate biological systems. Protected amino acids were utilized to more accurately mimic protein interactions and to avoid the improbable bidentate or even tridentate chelation that could occur with unprotected amino acids. **2a** and **2c** were therefore treated with an equimolar mixture (1 : 1 : 1) of Ac-Met-OMe, Ac-His-OMe and Ac-Cys-OMe for 24 h at rt and analyzed *via* $^1$H-NMR (1 mM; 10% d-DMF in D$_2$O) and HRMS (5 μM; 1% DMF in 400 μM NH$_4$OAc-solution). Additionally, the ruthena-
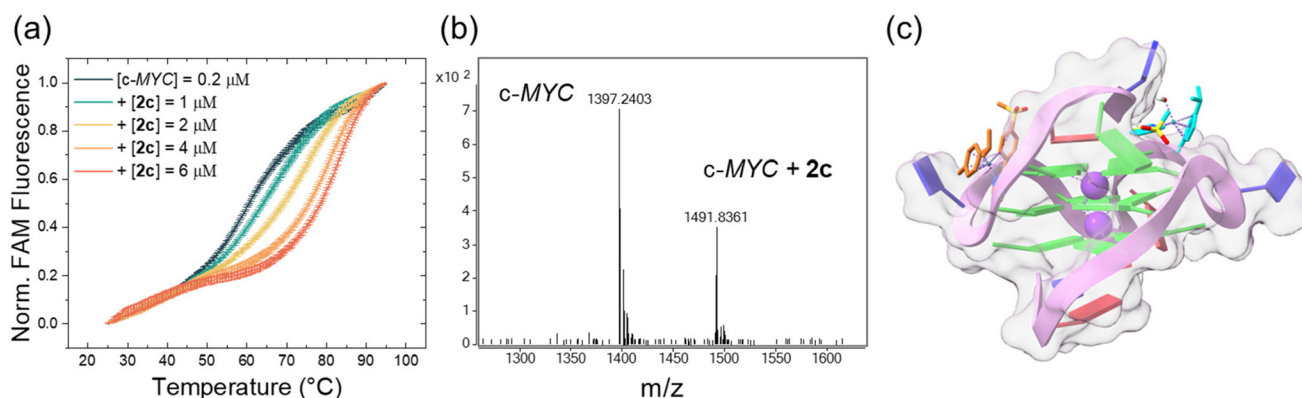


**Fig. 3** (a) FRET melting profiles of c-*MYC* (0.2 μM) upon interaction with **2c** at the indicated concentration values. (b) MS of **2c** incubated with c-*MYC* for 2 h at room temperature. Five charged masses of c-*MYC*: found: 1397.2403, calced: 1397.2318 (M–H$^-$ for C$_{220}$H$_{270}$O$_{131}$N$_{95}$P$_{21}$.) Five charged masses of **2c**-c-*MYC* adduct: found: 1491.8361, calced: 1491.8332 (M − H$^-$ for C$_{220}$H$_{270}$ O$_{131}$ N$_{95}$P$_{21}$C$_{20}$H$_{21}$NO$_2$RuS$_2$) (c) cartoon showing possible binding sites of **2c** (R) with c-*MYC* G4 (PDB id: 1XAV).

cycles were incubated with equimolar amounts of each amino acid individually and analyzed *via* the above described ^{1}H-NMR method.

Overall, unsubstituted **2a** reacted quantitatively with L-methionine and L-cysteine and only in the case of L-histidine small amounts of unreacted complex were present after 24 h according to NMR, whereby the L-methionine and L-histidine adducts were formed. However, due to the strong *trans* effect of thiols the complex decomposed after incubation with L-cysteine, releasing bidentate ligand **1a** (Fig. S59†). The mass spectrum validated that argument, as only the L-methionine-**2a** and L-histidine-**2a** adducts were observed (Fig. 4). Mesyl bearing **2c** proved to be less reactive since only traces of the L-methionine-**2c** and L-histidine-**2c** adducts were found by MS. This trend was also observed in the performed NMR experiments, where substantial amounts of **2c** remained unaltered after 24 h of incubation with each amino acid. Here again, only L-methionine and L-histidine adducts were recorded, while interaction with L-cysteine led to the mentioned loss of bidentate ligand **1c** (Fig. S60†). The competitive NMR experiments showed that for both complexes (**2a** and **2c**) the L-methionine adducts are preferably formed. In case of **2a**, a substantial amount of free bidentate ligand **1a** was observed.

**Cell cycle investigation.** Compounds **2c,d** and **3c,d** were examined for their ability to induce perturbations in the cell cycle of SW480 cells by means of propidium iodide staining, followed by flow cytometric analysis. The cells were investigated after 24 h exposure to the corresponding near-IC$_{50}$ concentrations (0.5×; 1×; 2× of 96 h IC$_{50}$).

In tested concentrations, the compounds exhibit minor to moderate effects on the cell cycle of SW480 cells (Table S13†). No clear concentration-effect pattern can be observed. However, there is a tendency of redistribution from the resting (G1/G0) phase towards the synthetic (S) and division (G2/M) phases, which might indicate a modest (*ca.* 10 ± 5%) but visible inhibition of the cell cycle in the latter two phases (Fig. S61 and S62†). Altogether, the mesyl bearing complexes

**2c** and **3c** induce stronger cell cycle perturbations at IC$_{50}$ levels, resulting in a 10–16% decrease of cells in G1/G0 phase. Interestingly, the Ru complex **2c** induces a redistribution of cells to G2/M phase (by *ca.* 12%), while the Os analog **3c** induces an S-phase inhibition (by *ca.* 14%) relative to the untreated control (Fig. S63†).

**Apoptosis/necrosis induction.** Compounds **2c,d** and **3c,d** were examined for their ability to induce apoptosis in SW480 cells by annexin V-FITC and propidium iodide double staining, followed by flow cytometric analysis. Since after 24 h hardly any apoptotic or necrotic effects were observed at relevant concentrations, the cells were incubated for 48 h in a second approach (Table S14 and Fig. S64†).

Surprisingly, the compounds only exhibit slight apoptotic effects, except for excessively high concentrations (≥100 μM). Osmium compounds **3c** and **3d** show the strongest induction of apoptosis after 48 h with 25% and 14%, respectively, at concentrations twice as high as their individual IC$_{50}$ values. Apoptotic potencies decrease in the following order: **3c** > **3d** > **2c** > **2d**, with the ruthenacycle **2d** only showing 5% of induced cell death at the stated concentration and incubation time. Generally, induction of cell death occurred slowly, as the fraction of early apoptotic cells is the largest, even after 48 h of incubation.

# Experimental part

## Materials and methods

Methanol was distilled from Mg/I$_2$ and stored over molecular sieve (3 Å). 4-Bromothiazole (98%, Ambeed), (4-fluorophenyl) boronic acid (TCI Europe), 4,4,5,5-tetramethyl-2-phenyl-1,3,2-dioxaborolane (98%, TCI Europe), 2-(4-methoxyphenyl)-4,4,5,5-tetramethyl-1,3,2-dioxaborolane (97%, Ambeed), 4,4,5,5-tetramethyl-2-(*p*-tolyl)-1,3,2-dioxaborolane (98%, Ambeed), (4-(methyl-(methylene)sulfinyl)phenyl)boronic acid (98%, Ambeed), potassium carbonate (Acros Fisher), tetrakis(triphenylphosphine)palladium(0) (>97%, TCI Europe), 1,4-dioxane (99.5%, Acros Fisher), ruthenium(III) chloride hydrate (38–41% Ru, Johnson Matthey), osmium tetroxide (Johnson Matthey), hydrazine dihydrochloride (≥98.0%, Sigma), α-terpinene (90%, Acros Fisher), sodium acetate anhydrous (≥98.5%, Fluka), potassium chloride (puriss, Molar Chemicals), disodium hydrogen phosphate (puriss, Molar Chemicals), sodium dihydrogen phosphate (puriss, Molar Chemicals), D$_2$O (99.9%, Sigma Aldrich), molecular sieve (3 Å, beads, 4–8 mesh), phosphate buffered saline (pH 7.4, 10×, Gibco), Ac-L-Met-OMe (97%, Ambeed), Ac-L-His-OMe (95%, Ambeed), Ac-L-Cys-OMe (97%, Ambeed) were used without further purification. The dimeric metal precursors [Ru(*p*-cymene)Cl$_2$]$_2$ and [Os(*p*-cymene)Cl$_2$]$_2$ were synthesized as described by Geisler *et al.*[46] Ligand **1a** was synthesized according to literature and ligands **1b–e** were obtained similarly. Acquired spectroscopic data of the ligands **1a–e** was in agreement with reported values.[47]

Purification *via* flash column chromatography was conducted with Biotage® Isolera system and silica gel (VWR,
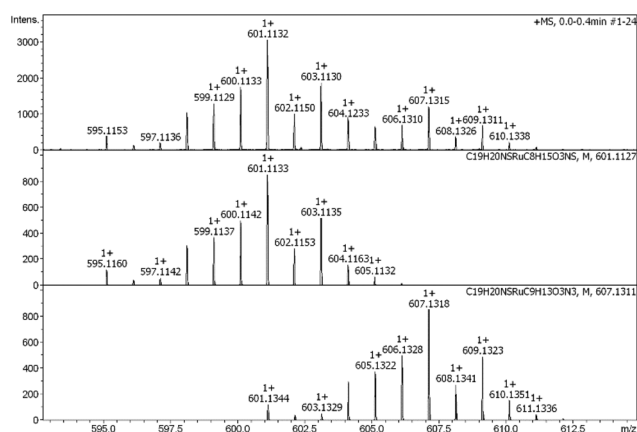


**Fig. 4** Mass spectrum of amino acid adducts (Ac-Met-OMe, Ac-His-OMe) of **2a**. First row: observed mass; second row: calculated mass for Met-adduct; third row: calculated mass for His-adduct.

mesh 40–63 μm). ¹H-, ¹³C- and 2D-NMR spectra of the complexes were recorded on a Bruker FT-NMR spectrometer Avance III™ HD 700.40 MHz or on a Bruker FT-NMR spectrometer Avance III™ 600.25 MHz, ¹H-NMR spectra of the ligands and amino acid interaction studies were recorded on a Bruker FT-NMR spectrometer AV NEO 500.10 MHz in CDCl₃ or D₂O and referenced to the residual solvent signals. High resolution ESI mass spectra of the metalacycles and amino acid interaction studies were recorded at the Mass Spectrometry Center of the University of Vienna (Faculty of Chemistry) on a Bruker maXis ESI-Qq-TOF Mass Spectrometer. High resolution mass spectra of 9-ethylguanine and oligonucleotide interactions were recorded on an Agilent 6540 QTOF LC/MS. Single crystal X-ray diffraction data were collected with a STOE STADIVARI Eulerian 4-circle diffractometer (STOE & CIE GmbH, Germany) equipped with an EIGER2 R500 detector (Dectris Ltd, Switzerland). Data were integrated with X-Area Integrate 2.5.3.0 (STOE, 2021) and scaled with X-Area LANA 2.7.5.0 (STOE, 2022). Structures were solved with SHELXS or SHELXT[48] and refined with SHELXL[49] in the GUI of Olex2.[50] Model building was done with Olex2 or ShelXle.[51] The structure were validated with CHECKCIF (https://checkcif.iucr.org/). Experimental data and CCDC-Codes Experimental data (available online: https://www.ccdc.cam.ac.uk/conts/retrieving.html) can be found in Table S1.† Crystal data, data collection parameters, and structure refinement details are reported in Tables S2–S8.† Structures, packing, interactions, and data are visualized in Fig. S1–S8.† Elemental analyses were performed by the Microanalytical Laboratory of the University of Vienna with a Eurovector EA 3000(2009) equipped with a high temperature pyrolysis furnace (HT, Hekatech, Germany, 2009). Elemental analyses samples were weighed on a Sartorius SEC 2 ultra-micro balance with ±0.1 μg resolution. Sample weights from 1–3 mg were used. For calibration two NIST-certified reference materials were used: sulfanilamide (C₆H₈N₂O₂S) and BBOT (2,5-bis-(5-tert-butyl-2-benzoxazol-2-yl)-thiophenone, C₂₆H₂₆N₂O₂S). The limit of quantification (LOQ) was 0.05 wt% for C, H, N and 0.02 wt% for S. The presented values are the average of determinations in triplicate. UV-Vis data were recorded on a PerkinElmer Lambda 650 UV-Vis Spectrophotometer with a Peltier element for temperature control. FRET experiments were performed at the AteN Center–Università di Palermo using a Applied Biosystems™ QuantStudio 6 PCR cycler.

**General complexation procedure.** Dimeric metal precursor (1.0 eq.), anhydrous NaOAc (4.0 eq.) and the respective 4-phenylthiazole (2.0 eq.) were dissolved in dry MeOH and stirred for 24 h at rt under Ar atmosphere. Subsequently, the solvent was evaporated, the residue was taken up in DCM and the suspension was filtered. Brine was added to the DCM solution and the mixture was stirred vigorously for 2 h. Afterwards the layers were separated, and the aqueous layer was extracted with DCM. The combined organic extracts were dried over anhydrous Na₂SO₄, filtered and the solvent was removed in vacuo. Purification was achieved via column chromatography on silica (60–80% EtOAc in n-hexane) utilizing a Biotage®

Isolera system, yielding the desired metalacycles in elemental analysis purity after drying for 2 days at 50 °C in vacuo.

**[(Chlorido)(4-phenylthiazolato-κN,κC2′)(η⁶-p-cymene)ruthenium(ɪɪ)] (2a).** The synthesis was performed according to the general complexation procedure, using [Ru(p-cym)Cl₂]₂ (100 mg, 163 μmol), 4-phenylthiazole (**1a**) (53 mg, 327 μmol) and anhydrous NaOAc (54 mg, 653 μmol) in dry MeOH (10 mL) for a reaction time of 20 h (10 g SiO₂, 65% EtOAc in n-hexane; 89 mg, 63%). ESI-HR-MS⁺ m/z found (calculated): [M − Cl]⁺ 396.0360 (396.0359), [M + Na]⁺ 453.9939 (453.9942). Elemental analysis found (calculated) for C₁₉H₂₀ClNRuS· 0.5H₂O: C 51.51 (51.87), H 4.62 (4.81), N 3.04 (3.18), S 6.92 (7.29), O 1.86 (1.82). ¹H NMR (600 MHz, CDCl₃): δ = 9.21 (d, ⁴J$_{H,H}$ = 2 Hz, 1H, ArH$_{Th-2}$), 8.11 (d, ³J$_{H,H}$ = 8 Hz, 1H, ArH$_{Ph-3}$), 7.42 (d, ³J$_{H,H}$ = 7 Hz, 1H, ArH$_{Ph-6}$), 7.30 (d, ⁴J$_{H,H}$ = 2 Hz, 1H, ArH$_{Th-5}$), 7.15 (ddd, ³J$_{H,H}$ = 7 Hz, ³J$_{H,H}$ = 7 Hz, ⁴J$_{H,H}$ = 1 Hz, 1H, ArH$_{Ph-4}$), 7.00 (dd, ³J$_{H,H}$ = 7 Hz, ³J$_{H,H}$ = 7 Hz, 1H, ArH$_{Ph-5}$), 5.58–5.53 (m, 2H, ArH$_{Cym-h}$, ArH$_{Cym-g}$), 5.21 (d, ³J$_{H,H}$ = 6 Hz, 1H, ArH$_{Cym-f}$), 5.02 (d, ³J$_{H,H}$ = 6 Hz, 1H, ArH$_{Cym-e}$), 2.41 (hept, ³J$_{H,H}$ = 7 Hz, 1H, CH$_{Cym-c}$), 2.03 (s, 3H, CH₃ $_{Cym-d}$), 0.96 (d, ³J$_{H,H}$ = 7 Hz, 3H, CH₃ $_{Cym-b}$), 0.92 (d, ³J$_{H,H}$ = 7 Hz, 3H, CH₃ $_{Cym-a}$) ppm. ¹³C NMR (151 MHz, CDCl₃): δ = 175.3 (C$_{Ph-2}$), 163.4 (C$_{Th-5}$), 153.3 (C$_{Th-2}$), 139.8 (C$_{Ph-3}$), 137.9 (C$_{Ph-1}$), 128.7 (C$_{Ph-4}$), 123.0 (C$_{Ph-5}$), 122.5 (C$_{Ph-6}$), 107.7 (C$_{Th-4}$), 100.0 (C$_{Cym-1}$), 99.8 (C$_{Cym-6}$), 89.3 (C$_{Cym-h}$), 88.4 (C$_{Cym-g}$), 83.9 (C$_{Cym-f}$), 82.0 (C$_{Cym-e}$), 30.9 (C$_{Cym-c}$), 22.5 (C$_{Cym-b}$), 22.0 (C$_{Cym-a}$), 18.9 (C$_{Cym-d}$) ppm.

**[(Chlorido)(4-(4-fluorophenyl)thiazolato-κN,κC2′)(η⁶-p-cymene)ruthenium(ɪɪ)] (2b).** The synthesis was performed according to the general complexation procedure, using [Ru(p-cym)Cl₂]₂ (200 mg, 327 μmol), 4-(4-fluorophenyl)thiazole (**1b**) (117 mg, 653 μmol) and anhydrous NaOAc (107 mg, 1.31 mmol) in dry MeOH (20 mL) for a reaction time of 22 h (25 g SiO₂, 65% EtOAc in n-hexane; 253 mg, 86%). ESI-HR-MS⁺ m/z found (calculated): [M − Cl]⁺ 414.0264 (414.0265), [M + Na]⁺ 471.9843 (471.9848). Elemental analysis found (calculated) for C₁₉H₁₉ClFNRuS·0.25H₂O: C 50.04 (50.33), H 4.17 (4.33), N 3.06 (3.09), S 7.15 (7.07), O 1.06 (0.88). ¹H NMR (700.40 MHz, CDCl₃): δ = 9.19 (d, ⁴J$_{H,H}$ = 2 Hz, 1H, ArH$_{Th-2}$), 7.79 (dd, ³J$_{H,F}$ = 9 Hz, ⁴J$_{H,H}$ = 3 Hz, 1H, ArH$_{Ph-3}$), 7.40 (dd, ³J$_{H,H}$ = 8 Hz, ⁴J$_{H,F}$ = 5 Hz, 1H, ArH$_{Ph-6}$), 7.23 (d, ⁴J$_{H,H}$ = 2 Hz, 1H, ArH$_{Th-5}$), 6.69 (ddd, ³J$_{H,F}$ = 9 Hz, ³J$_{H,F}$ = 9 Hz, ⁴J$_{H,H}$ = 3 Hz, 1H, ArH$_{Ph-5}$), 5.56 (d, ³J$_{H,H}$ = 6 Hz, 1H, ArH$_{Cym-h}$), 5.54 (d, ³J$_{H,H}$ = 6 Hz, 1H, ArH$_{Cym-g}$), 5.22 (d, ³J$_{H,H}$ = 6 Hz, 1H, ArH$_{Cym-f}$), 5.02 (d, ³J$_{H,H}$ = 6 Hz, 1H, ArH$_{Cym-e}$), 2.41 (hept, ³J$_{H,H}$ = 7 Hz, 1H, CH$_{Cym-c}$), 2.05 (s, 3H, CH₃ $_{Cym-d}$), 0.96 (d, ³J$_{H,H}$ = 7 Hz, 3H, CH₃ $_{Cym-b}$), 0.92 (d, ³J$_{H,H}$ = 7 Hz, 3H, CH₃ $_{Cym-a}$) ppm. ¹³C NMR (176.12 MHz, CDCl₃): δ = 178.1 (d, ³J$_{C,F}$ = 4 Hz, C$_{Ph-2}$), 162.4 (C$_{Th-5}$), 162.1 (d, ¹J$_{C,F}$ = 252 Hz, C$_{Ph-4}$), 153.5 (C$_{Th-2}$), 134.2 (d, ⁴J$_{C,F}$ = 2 Hz, C$_{Ph-1}$), 125.6 (d, ²J$_{C,F}$ = 17 Hz, C$_{Ph-3}$), 123.4 (d, ²J$_{C,F}$ = 8 Hz, C$_{Ph-6}$), 110.2 (d, ³J$_{C,F}$ = 23 Hz, C$_{Ph-5}$), 107.2 (d, ⁵J$_{C,F}$ = 1 Hz, C$_{Th-4}$), 100.4 (C$_{Cym-1}$), 100.3 (C$_{Cym-6}$), 89.4 (C$_{Cym-h}$), 88.4 (C$_{Cym-g}$), 84.2 (C$_{Cym-f}$), 82.2 (C$_{Cym-e}$), 30.9 (C$_{Cym-c}$), 22.5 (C$_{Cym-b}$), 22.0 (C$_{Cym-a}$), 18.9 (C$_{Cym-d}$) ppm.

**[(Chlorido)(4-(4-(methylsulfonyl)phenyl)thiazolato-κN,κC2′)(η⁶-p-cymene)ruthenium(ɪɪ)] (2c).** The synthesis was performed

according to the general complexation procedure, using [Ru(*p*-cym)Cl$_2$]$_2$ (200 mg, 327 µmol), 4-(4-(methylsulfonyl)phenyl)thiazole (**1c**) (156 mg, 653 µmol) and anhydrous NaOAc (107 mg, 1.31 mmol) in dry MeOH (20 mL) for a reaction time of 22 h (25 g SiO$_2$, 100% EtOAc; 164 mg, 49%). ESI-HR-MS$^+$ *m/z* found (calculated): [M − Cl]$^+$ 474.0134 (474.0134), [M + Na]$^+$ 531.9714 (531.9717). Elemental analysis found (calculated) for C$_{20}$H$_{22}$ClNO$_2$RuS$_2$·0.25C$_4$H$_8$O$_2$·0.30H$_2$O: C 46.66 (47.01), H 4.36 (4.62), N 2.74 (2.61), S 11.70 (11.95), O 8.29 (8.35). $^1$H NMR (700.40 MHz, CDCl$_3$): δ = 9.26 (d, $^4J_{H,H}$ = 2 Hz, 1H, ArH$_{Th-2}$), 8.63 (d, $^4J_{H,H}$ = 1 Hz, 1H, ArH$_{Ph-3}$), 7.58–7.52 (m, 3H, ArH$_{Ph-5}$, ArH$_{Ph-6}$, ArH$_{Th-5}$), 5.65 (d, $^3J_{H,H}$ = 6 Hz, 1H, ArH$_{Cym-h}$), 5.62 (d, $^3J_{H,H}$ = 6 Hz, 1H, ArH$_{Cym-g}$), 5.25 (d, $^3J_{H,H}$ = 6 Hz, 1H, ArH$_{Cym-f}$), 5.06 (d, $^3J_{H,H}$ = 6 Hz, 1H, ArH$_{Cym-e}$), 3.09 (s, 3H, CH$_3$ $_{SO_2Me}$), 2.38 (hept, $^3J_{H,H}$ = 7 Hz, 1H, CH$_{Cym-c}$), 2.07 (s, 3H, CH$_3$ $_{Cym-d}$), 0.95 (d, $^3J_{H,H}$ = 7 Hz, 3H, CH$_3$ $_{Cym-b}$), 0.88 (d, $^3J_{H,H}$ = 7 Hz, 3H, CH$_3$ $_{Cym-a}$) ppm. $^{13}$C NMR (176.12 MHz, CDCl$_3$): δ = 176.9 (C$_{Ph-2}$), 161.6 (C$_{Th-5}$), 154.2 (C$_{Th-2}$), 143.0 (C$_{Ph-1}$), 138.8 (C$_{Ph-4}$), 137.7 (C$_{Ph-3}$), 122.4 (C$_{Ph-5}$), 122.2 (C$_{Ph-6}$), 111.3 (C$_{Th-4}$), 101.7 (C$_{Cym-6}$), 100.9 (C$_{Cym-1}$), 89.7 (C$_{Cym-h}$), 88.7 (C$_{Cym-g}$), 84.3 (C$_{Cym-f}$), 81.7 (C$_{Cym-e}$), 45.0 (C$_{SO_2Me}$), 30.9 (C$_{Cym-c}$), 22.6 (C$_{Cym-b}$), 22.0 (C$_{Cym-a}$), 19.0 (C$_{Cym-d}$) ppm.

**[(Chlorido)(4-(4-methylphenyl)thiazolato-κN,κC2′)(η$^6$-*p*-cymene)ruthenium(ɪɪ)] (2d).** The synthesis was performed according to the general complexation procedure, using [Ru(*p*-cym)Cl$_2$]$_2$ (200 mg, 327 µmol), 4-(4-methylphenyl)thiazole (**1d**) (114 mg, 653 µmol) and anhydrous NaOAc (107 mg, 1.31 mmol) in dry MeOH (20 mL) for a reaction time of 22 h (25 g SiO$_2$, 65% EtOAc in *n*-hexane; 168 mg, 58%). ESI-HR-MS$^+$ *m/z* found (calculated): [M − Cl]$^+$ 410.0510 (410.0516), [M + Na]$^+$ 468.0091 (468.0099). Elemental analysis found (calculated) for C$_{20}$H$_{22}$ClNRuS·0.25H$_2$O: C 53.62 (53.44), H 4.89 (5.05), N 3.17 (3.12), S 6.76 (7.13), O 0.99 (0.89). $^1$H NMR (700.40 MHz, CDCl$_3$): δ = 9.19 (d, $^4J_{H,H}$ = 2 Hz, 1H, ArH$_{Th-2}$), 7.93 (s, 1H, ArH$_{Ph-3}$), 7.32 (d, $^3J_{H,H}$ = 8 Hz, 1H, ArH$_{Ph-6}$), 7.22 (d, $^4J_{H,H}$ = 2 Hz, 1H, ArH$_{Th-5}$), 6.81 (dd, $^3J_{H,H}$ = 8 Hz, $^4J_{H,H}$ = 1 Hz, 1H, ArH$_{Ph-5}$), 5.56 (d, $^3J_{H,H}$ = 6 Hz, 1H, ArH$_{Cym-h}$), 5.53 (d, $^3J_{H,H}$ = 6 Hz, 1H, ArH$_{Cym-g}$), 5.23 (d, $^3J_{H,H}$ = 6 Hz, 1H, ArH$_{Cym-f}$), 5.02 (d, $^3J_{H,H}$ = 6 Hz, 1H, ArH$_{Cym-e}$), 2.42–2.35 (m, 4H, CH$_3$ $_{Ph}$, CH$_{Cym-c}$), 2.03 (s, 3H), 0.95 (d, $^3J_{H,H}$ = 7 Hz, 3H, CH$_3$ $_{Cym-b}$), 0.92 (d, $^3J_{H,H}$ = 7 Hz, 3H, CH$_3$ $_{Cym-a}$) ppm. $^{13}$C NMR (176.12 MHz, CDCl$_3$): δ = 175.2 (C$_{Ph-2}$), 163.4 (C$_{Th-5}$), 153.1 (C$_{Th-2}$), 140.3 (C$_{Ph-3}$), 138.2 (C$_{Ph-4}$), 135.3 (C$_{Ph-1}$), 124.1 (C$_{Ph-5}$), 122.2 (C$_{Ph-6}$), 106.7 (C$_{Th-4}$), 99.6 (C$_{Cym-1}$), 99.5 (C$_{Cym-6}$), 89.5 (C$_{Cym-h}$), 88.1 (C$_{Cym-g}$), 84.2 (C$_{Cym-f}$), 81.9 (C$_{Cym-e}$), 30.9 (C$_{Cym-c}$), 22.4 (C$_{Cym-b}$), 22.2 (C$_{Cym-a}$), 22.0 (C$_{CH_3}$), 18.9 (C$_{Cym-d}$) ppm.

**[(Chlorido)(4-(4-methoxyphenyl)thiazolato-κN,κC2′)(η$^6$-*p*-cymene)ruthenium(ɪɪ)] (2e).** The synthesis was performed according to the general complexation procedure, using [Ru(*p*-cym)Cl$_2$]$_2$ (200 mg, 327 µmol), 4-(4-methoxyphenyl)thiazole (**1e**) (125 mg, 653 µmol) and anhydrous NaOAc (107 mg, 1.31 mmol) in dry MeOH (20 mL) for a reaction time of 22 h (25 g SiO$_2$, 65% EtOAc in *n*-hexane; 173 mg, 57%). ESI-HR-MS$^+$ *m/z* found (calculated): [M − Cl]$^+$ 426.0466 (426.0465), [M + Na]$^+$ 484.0046 (484.0048). Elemental analysis found (calculated) for C$_{20}$H$_{22}$ClNORuS·0.25H$_2$O: C 51.36 (51.60), H 4.59

(4.87), N 3.12 (3.01), S 6.66 (6.89), O 4.32 (4.30). $^1$H NMR (700.40 MHz, CDCl$_3$): δ = 9.17 (d, $^4J_{H,H}$ = 2 Hz, 1H, ArH$_{Th-2}$), 7.67 (d, $^4J_{H,H}$ = 2 Hz, 1H, ArH$_{Ph-3}$), 7.37 (d, $^3J_{H,H}$ = 8 Hz, 1H, ArH$_{Ph-6}$), 7.13 (d, $^4J_{H,H}$ = 2 Hz, 1H, ArH$_{Th-5}$), 6.57 (dd, $^3J_{H,H}$ = 8 Hz, $^4J_{H,H}$ = 3 Hz, 1H, ArH$_{Ph-5}$), 5.54 (d, $^3J_{H,H}$ = 6 Hz, 2H, ArH$_{Cym-h}$, ArH$_{Cym-g}$), 5.21 (d, $^3J_{H,H}$ = 6 Hz, 1H, ArH$_{Cym-f}$), 5.02 (d, $^3J_{H,H}$ = 6 Hz, 1H, ArH$_{Cym-e}$), 3.89 (s, 3H, CH$_3$ $_{OMe}$), 2.42 (hept, $^3J_{H,H}$ = 7 Hz, 1H, CH$_{Cym-c}$), 2.03 (s, 3H, CH$_3$ $_{Cym-c}$), 0.96 (d, $^3J_{H,H}$ = 7 Hz, 3H, CH$_3$ $_{Cym-b}$), 0.92 (d, $^3J_{H,H}$ = 7 Hz, 3H, CH$_3$ $_{Cym-a}$) ppm. $^{13}$C NMR (176.12 MHz, CDCl$_3$): δ = 177.1 (C$_{Ph-2}$), 163.1 (C$_{Th-5}$), 159.1 (C$_{Ph-4}$), 153.1 (C$_{Th-2}$), 131.4 (C$_{Ph-1}$), 124.6 (C$_{Ph-3}$), 123.2 (C$_{Ph-6}$), 108.7 (C$_{Ph-5}$), 105.5 (C$_{Th-4}$), 99.9 (C$_{Cym-1}$), 99.6 (C$_{Cym-6}$), 89.2 (C$_{Cym-h}$), 88.4 (C$_{Cym-g}$), 84.1 (C$_{Cym-f}$), 82.3 (C$_{Cym-e}$), 55.3 (C$_{CH_3}$), 30.9 (C$_{Cym-c}$), 22.5 (C$_{Cym-b}$), 22.0 (C$_{Cym-a}$), 18.9 (C$_{Cym-d}$) ppm.

**[(Chlorido)(4-phenylthiazolato-κN,κC2′)(η$^6$-*p*-cymene)osmium(ɪɪ)] (3a).** The synthesis was performed according to the general complexation procedure, using [Os(*p*-cym)Cl$_2$]$_2$ (400 mg, 506 µmol), 4-phenylthiazole (**1a**) (163 mg, 1.01 mmol) and anhydrous NaOAc (166 mg, 2.02 mmol) in dry MeOH (40 mL) for a reaction time of 21 h (25 g SiO$_2$, 65% EtOAc in *n*-hexane; 389 mg, 74%). ESI-HR-MS$^+$ *m/z* found (calculated): [M − Cl]$^+$ 486.0927 (486.0924), [M + Na]$^+$ 544.0502 (544.0500). Elemental analysis found (calculated) for C$_{19}$H$_{20}$ClNOsS·0.25H$_2$O: C 43.58 (43.50), H 3.77 (3.94), N 2.73 (2.67), S 6.09 (6.11), O 0.69 (0.76). $^1$H NMR (600.25 MHz, CDCl$_3$): δ = 9.08 (d, $^4J_{H,H}$ = 2 Hz, 1H, ArH$_{Th-2}$), 7.96 (dd, $^3J_{H,H}$ = 8 Hz, $^4J_{H,H}$ = 1 Hz, 1H, ArH$_{Ph-3}$), 7.48 (dd, $^3J_{H,H}$ = 8 Hz, $^4J_{H,H}$ = 1 Hz, 1H, ArH$_{Ph-6}$), 7.29 (d, $^4J_{H,H}$ = 2 Hz, 1H, ArH$_{Th-5}$), 7.11 (ddd, $^3J_{H,H}$ = 7 Hz, $^3J_{H,H}$ = 7 Hz, $^4J_{H,H}$ = 1 Hz, 1H, ArH$_{Ph-4}$), 6.98 (ddd, $^3J_{H,H}$ = 7 Hz, $^3J_{H,H}$ = 7 Hz, $^4J_{H,H}$ = 1 Hz, 1H, ArH$_{Ph-5}$), 5.57 (d, $^3J_{H,H}$ = 5 Hz, 1H, ArH$_{Cym-g}$), 5.53 (d, $^3J_{H,H}$ = 6 Hz, 1H, ArH$_{Cym-h}$), 5.39 (d, $^3J_{H,H}$ = 6 Hz, 1H, ArH$_{Cym-f}$), 5.23 (d, $^3J_{H,H}$ = 5 Hz, 1H, ArH$_{Cym-e}$), 2.34 (hept, $^3J_{H,H}$ = 7 Hz, 1H, CH$_{Cym-c}$), 2.15 (s, 3H, CH$_3$ $_{Cym-d}$), 0.97 (d, $^3J_{H,H}$ = 7 Hz, 3H, CH$_3$ $_{Cym-b}$), 0.90 (d, $^3J_{H,H}$ = 7 Hz, 3H, CH$_3$ $_{Cym-a}$) ppm. $^{13}$C NMR (150.93 MHz, CDCl$_3$): δ = 166.0 (C$_{Th-5}$), 162.2 (C$_{Ph-2}$), 153.2 (C$_{Th-2}$), 139.7 (C$_{Ph-3}$), 138.4 (C$_{Ph-1}$), 129.3 (C$_{Ph-4}$), 123.0 (C$_{Ph-5}$), 122.3 (C$_{Ph-6}$), 107.7 (C$_{Th-4}$), 92.7 (C$_{Cym-6}$), 90.5 (C$_{Cym-1}$), 79.5 (C$_{Cym-h}$), 78.9 (C$_{Cym-g}$), 74.9 (C$_{Cym-f}$), 71.9 (C$_{Cym-e}$), 31.1 (C$_{Cym-c}$), 22.8 (C$_{Cym-b}$), 22.3 (C$_{Cym-a}$), 18.7 (C$_{Cym-d}$) ppm.

**[(Chlorido)(4-(4-fluorophenyl)thiazolato-κN,κC2′)(η$^6$-*p*-cymene)osmium(ɪɪ)] (3b).** The synthesis was performed according to the general complexation procedure, using [Os(*p*-cym)Cl$_2$]$_2$ (200 mg, 253 µmol), 4-(4-fluorophenyl)thiazole (**1b**) (91 mg, 506 µmol) and anhydrous NaOAc (83 mg, 1.01 mmol) in dry MeOH (20 mL) for a reaction time of 22 h (25 g SiO$_2$, 60% EtOAc in *n*-hexane; 126 mg, 46%). ESI-HR-MS$^+$ *m/z* found (calculated): [M − Cl]$^+$ 504.0824 (504.0830), [M + Na]$^+$ 562.0401 (562.0406). Elemental analysis found (calculated) for C$_{19}$H$_{19}$ClFNOsS·0.25H$_2$O: C 42.31 (42.06), H 3.57 (3.62), N 2.64 (2.58), S 5.99 (5.91), O 0.62 (0.74). $^1$H NMR (600.25 MHz, CDCl$_3$): δ = 9.06 (d, $^4J_{H,H}$ = 2 Hz, 1H, ArH$_{Th-2}$), 7.63 (dd, $^3J_{H,F}$ = 10 Hz, $^4J_{H,H}$ = 3 Hz, 1H, ArH$_{Ph-3}$), 7.46 (dd, $^3J_{H,H}$ = 8 Hz, $^4J_{H,F}$ = 5 Hz, 1H, ArH$_{Ph-6}$), 7.22 (d, $^4J_{H,H}$ = 2 Hz, 1H, ArH$_{Th-5}$), 6.68 (ddd, $^3J_{H,F}$ = 9 Hz, $^3J_{H,F}$ = 9 Hz, $^4J_{H,H}$ = 3 Hz, 1H, ArH$_{Ph-5}$), 5.56

(d, $^3J_{H,H}$ = 5 Hz, 1H, ArH$_{Cym-g}$), 5.53 (d, $^3J_{H,H}$ = 5 Hz, 1H, ArH$_{Cym-h}$), 5.39 (d, $^3J_{H,H}$ = 5 Hz, 1H, ArH$_{Cym-f}$), 5.22 (d, $^3J_{H,H}$ = 5 Hz, 1H, ArH$_{Cym-e}$), 2.35 (hept, $^3J_{H,H}$ = 7 Hz, 1H, CH$_{Cym-c}$), 2.17 (s, 3H CH$_{3\ Cym-d}$), 0.97 (d, $^3J_{H,H}$ = 7 Hz, 3H, CH$_{3\ Cym-b}$), 0.90 (d, $^3J_{H,H}$ = 7 Hz, 3H, CH$_{3\ Cym-a}$) ppm. $^{13}$C NMR (150.93 MHz, CDCl$_3$): $\delta$ = 164.9 (C$_{Th-5}$), 164.8 (d, $^3J_{C,F}$ = 5 Hz, C$_{Ph-2}$), 163.0 (d, $^1J_{C,F}$ = 251 Hz, C$_{Ph-4}$), 153.5 (C$_{Th-2}$), 134.7 (d, $^4J_{C,F}$ = 2 Hz, C$_{Ph-1}$), 125.4 (d, $^2J_{C,F}$ = 18 Hz, C$_{Ph-3}$), 123.5 (d, $^3J_{C,F}$ = 9 Hz, C$_{Ph-6}$), 110.1 (d, $^2J_{C,F}$ = 23 Hz, C$_{Ph-5}$), 107.2 (C$_{Th-4}$), 93.4 (C$_{Ph-6}$), 90.9 (C$_{Ph-1}$), 79.6 (C$_{Cym-h}$), 78.9 (C$_{Cym-g}$), 75.2 (C$_{Cym-f}$), 72.1 (C$_{Cym-e}$), 31.1(C$_{Cym-c}$), 22.8 (C$_{Cym-b}$), 22.3 (C$_{Cym-a}$), 18.7 (C$_{Cym-d}$) ppm.

**[(Chlorido)(4-(4-(methylsulfonyl)phenyl)thiazolato-κN,κC2′) (η⁶-*p*-cymene)osmium(ɪɪ)] (3c).** The synthesis was performed according to the general complexation procedure, using [Os(*p*-cym)Cl$_2$]$_2$ (200 mg, 253 μmol), 4-(4-(methylsulfonyl)phenyl)thiazole (**1c**) (121 mg, 506 mmol) and anhydrous NaOAc (83 mg, 1.01 mmol) in dry MeOH (20 mL) for a reaction time of 22 h (25 g SiO$_2$, 75–85% EtOAc in *n*-hexane; 210 mg, 69%). ESI-HR-MS⁺ *m/z* found (calculated): [M − Cl]⁺ 564.0691 (564.0698), [M + Na]⁺ 622.0270 (622.0274). Elemental analysis found (calculated) for C$_{20}$H$_{22}$ClNO$_2$OsS$_2$·0.40H$_2$O: C 40.03 (39.68), H 3.65 (3.80), N 2.31 (2.31), S 10.25 (10.59), O 6.47 (6.34). $^1$H NMR (600.25 MHz, CDCl$_3$): $\delta$ = 9.13 (d, $^4J_{H,H}$ = 2 Hz, 1H, ArH$_{Th-2}$), 8.47 (d, $^4J_{H,H}$ = 2 Hz, 1H, ArH$_{Ph-3}$), 7.60 (d, $^3J_{H,H}$ = 8 Hz, 1H, ArH$_{Ph-6}$), 7.56–7.50 (m, 2H, ArH$_{Th-5}$, ArH$_{Ph-5}$), 5.65 (d, $^3J_{H,H}$ = 6 Hz, 1H, ArH$_{Cym-g}$), 5.61 (d, $^3J_{H,H}$ = 6 Hz, 1H, ArH$_{Cym-h}$), 5.42 (d, $^3J_{H,H}$ = 6 Hz, 1H, ArH$_{Cym-f}$), 5.27 (d, $^3J_{H,H}$ = 6 Hz, 1H, ArH$_{Cym-e}$), 3.08 (s, 3H, CH$_{3\ SO_2Me}$), 2.31 (hept, $^3J_{H,H}$ = 7 Hz, 1H, CH$_{Cym-c}$), 2.18 (s, 3H, CH$_{3\ Cym-d}$), 0.95 (d, $^3J_{H,H}$ = 7 Hz, 3H, CH$_{3\ Cym-b}$), 0.86 (d, $^3J_{H,H}$ = 7 Hz, 3H, CH$_{3\ Cym-a}$) ppm. $^{13}$C NMR (150.93 MHz, CDCl$_3$): $\delta$ = 164.2 (C$_{Th-5}$), 163.2 (C$_{Ph-2}$), 154.2 (C$_{Th-2}$), 143.5 (C$_{Ph-1}$), 139.3 (C$_{Ph-4}$), 137.8 (C$_{Ph-3}$), 122.4 (C$_{Ph-6}$), 122.1 (C$_{Ph-5}$), 111.3 (C$_{Th-4}$), 94.6 (C$_{Cym-6}$), 91.5 (C$_{Cym-1}$), 80.0 (C$_{Cym-h}$), 79.2 (C$_{Cym-g}$), 75.4 (C$_{Cym-f}$), 71.8 (C$_{Cym-e}$), 45.0 (C$_{SO_2Me}$), 31.1 (C$_{Cym-c}$), 22.9 (C$_{Cym-b}$), 22.2 (C$_{Cym-a}$), 18.7 (C$_{Cym-d}$) ppm.

**[(Chlorido)(4-(4-methylphenyl)thiazolato-κN,κC2′)(η⁶-*p*-cymene) osmium(ɪɪ)] (3d).** The synthesis was performed according to the general complexation procedure, using [Os(*p*-cym)Cl$_2$]$_2$ (400 mg, 506 μmol), 4-(4-methylphenyl)thiazole (**1d**) (177 mg, 1.01 mmol) and anhydrous NaOAc (166 mg, 2.02 mmol) in dry MeOH (40 mL) for a reaction time of 22 h (25 g SiO$_2$, 60% EtOAc in *n*-hexane; 411 mg, 76%). ESI-HR-MS⁺ *m/z* found (calculated): [M − Cl]⁺ 500.1086 (500.1081), [M + Na]⁺ 558.0658 (558.0656). Elemental analysis found (calculated) for C$_{20}$H$_{22}$ClNOsS·0.25H$_2$O: C 44.81 (44.60), H 3.98 (4.21), N 2.69 (2.60), S 5.99 (5.95), O 0.77 (0.74). $^1$H NMR (600.25 MHz, CDCl$_3$): $\delta$ = 9.06 (d, $^4J_{H,H}$ = 2 Hz, 1H, ArH$_{Th-2}$), 7.78 (s, 1H, ArH$_{Ph-3}$), 7.38 (d, $^3J_{H,H}$ = 8 Hz, 1H, ArH$_{Ph-6}$), 7.21 (d, $^4J_{H,H}$ = 2 Hz, 1H, ArH$_{Th-5}$), 6.80 (dd, $^3J_{H,H}$ = 8 Hz, $^4J_{H,H}$ = 2 Hz, 1H, ArH$_{Ph-5}$), 5.56 (d, $^3J_{H,H}$ = 5 Hz, 1H, ArH$_{Cym-g}$), 5.53 (d, $^3J_{H,H}$ = 6 Hz, 1H, ArH$_{Cym-h}$), 5.40 (d, $^3J_{H,H}$ = 6 Hz, 1H, ArH$_{Cym-f}$), 5.23 (d, $^3J_{H,H}$ = 5 Hz, 1H, ArH$_{Cym-e}$), 2.37–2.30 (m, 4H, CH$_{3\ Ph}$, CH$_{Cym-c}$), 2.16 (s, 3H, CH$_{3\ Cym-d}$), 0.96 (d, $^3J_{H,H}$ = 7 Hz, 3H, CH$_{3\ Cym-b}$), 0.91 (d, $^3J_{H,H}$ = 7 Hz, 3H, CH$_{3\ Cym-a}$) ppm. $^{13}$C NMR (150.93 MHz, CDCl$_3$): $\delta$ = 166.0 (C$_{Th-5}$), 162.2 (C$_{Ph-2}$), 153.0

(C$_{Th-2}$), 140.2 (C$_{Ph-3}$), 138.7 (C$_{Ph-4}$), 135.9 (C$_{Ph-1}$), 124.2 (C$_{Ph-5}$), 122.1 (C$_{Ph-6}$), 106.6 (C$_{Th-4}$), 92.5 (C$_{Cym-6}$), 90.2 (C$_{Cym-1}$), 79.6 (C$_{Cym-h}$), 78.6 (C$_{Cym-g}$), 75.2 (C$_{Cym-f}$), 71.7 (C$_{Cym-e}$), 31.1 (C$_{Cym-c}$), 22.8 (C$_{Cym-b}$), 22.4 (C$_{Cym-a}$), 21.9 (C$_{CH3}$), 18.7 (C$_{Cym-d}$) ppm.

**[(Chlorido)(4-(4-methoxyphenyl)thiazolato-κN,κC2′)(η⁶-*p*-cymene)osmium(ɪɪ)] (3e).** The synthesis was performed according to the general complexation procedure, using [Os(*p*-cym) Cl$_2$]$_2$ (400 mg, 506 μmol), 4-(4-methoxyphenyl)thiazole (**1e**) (194 mg, 1.01 mmol) and anhydrous NaOAc (166 mg, 2.02 mmol) in dry MeOH (40 mL) for a reaction time of 22 h (25 g SiO$_2$, 70% EtOAc in *n*-hexane; 389 mg, 74%). ESI-HR-MS⁺ *m/z* found (calculated): [M − Cl]⁺ 516.1032 (516.1030), [M + Na]⁺ 574.0607 (574.0606). Elemental analysis found (calculated) for C$_{20}$H$_{22}$ClNOOsS·0.25H$_2$O: C 43.47 (43.31), H 3.85 (4.09), N 2.59 (2.53), S 5.86 (5.78), O 3.79 (3.61). $^1$H NMR (600.25 MHz, CDCl$_3$): $\delta$ = 9.04 (d, $^4J_{H,H}$ = 2 Hz, 1H, ArH$_{Th-2}$), 7.51 (d, $^4J_{H,H}$ = 3 Hz, 1H, ArH$_{Ph-3}$), 7.43 (d, $^3J_{H,H}$ = 8 Hz, 1H, ArH$_{Ph-6}$), 7.12 (d, $^4J_{H,H}$ = 2 Hz, 1H, ArH$_{Th-5}$), 6.56 (dd, $^3J_{H,H}$ = 8 Hz, $^4J_{H,H}$ = 3 Hz, 1H, ArH$_{Ph-5}$), 5.56 (d, $^3J_{H,H}$ = 5.4 Hz, 1H, ArH$_{Cym-g}$), 5.51 (d, $^3J_{H,H}$ = 6 Hz, 1H, ArH$_{Cym-h}$), 5.39 (d, $^3J_{H,H}$ = 6 Hz, 1H, ArH$_{Cym-f}$), 5.22 (d, $^3J_{H,H}$ = 5 Hz, 1H, ArH$_{Cym-e}$), 3.87 (s, 3H, CH$_{3\ OMe}$), 2.35 (hept, $^3J_{H,H}$ = 7 Hz, 1H, CH$_{Cym-c}$), 2.15 (s, 3H, CH$_{3\ Cym-d}$), 0.97 (d, $^3J_{H,H}$ = 7 Hz, 3H, CH$_{3\ Cym-b}$), 0.91 (d, $^3J_{H,H}$ = 7 Hz, 3H, CH$_{3\ Cym-a}$) ppm. $^{13}$C NMR (150.93 MHz, CDCl$_3$): $\delta$ = 165.6 (C$_{Th-5}$), 163.9 (C$_{Ph-2}$), 159.8 (C$_{Ph-4}$), 153.0 (C$_{Th-2}$), 132.0 (C$_{Ph-1}$), 124.5 (C$_{Ph-3}$), 123.3 (C$_{Ph-6}$), 108.8 (C$_{Ph-5}$), 105.5 (C$_{Th-4}$), 92.6 (C$_{Cym-6}$), 90.5 (C$_{Cym-1}$), 79.4 (C$_{Cym-h}$), 78.9 (C$_{Cym-g}$), 75.1 (C$_{Cym-f}$), 72.1 (C$_{Cym-e}$), 55.2 (C$_{OMe}$), 31.1 (C$_{Cym-c}$), 22.9 (C$_{Cym-b}$), 22.3 (C$_{Cym-a}$), 18.7 (C$_{Cym-d}$) ppm.

**Stability in aqueous solution by UV-Vis spectroscopy.** Stock solutions (10 mM) in DMF were prepared and diluted with PBS (pH 7.4) to achieve a final concentration of 40 μM (1% DMF content). UV-Vis spectra were recorded in a 30 min interval for 24 h at 20 °C on a PerkinElmer Lambda 650 UV-Vis Spectrophotometer with a Peltier element for temperature control.

**Chloride ion affinity.** The chloride affinity was determined for **2a** and **2c** in UV-Vis spectrophotometric measurements, similar to the method reported formerly.[52] Individual samples were prepared with constant complex concentration (100 or 120 μM) and increasing KCl concentration (0–1 M). The one equivalent chloride ion originating from the complexes was included in our calculations. HypSpec was used to calculate the log $K'$(H$_2$O/Cl⁻) constants.[53]

**Amino acid interaction studies**

*ESI-MS.* Stock solutions in DMF were prepared and diluted with 400 μM NH$_4$OAc solution (pH 7.4) to achieve a final concentration of 5 μM (1% DMF content). The complex solution was subjected to incubation with a balanced mixture (1 : 1 : 1) of protected amino acids Ac-Cys-OMe, Ac-His-OMe and Ac-Met-OMe in 400 μM NH$_4$OAc (5 μM each). Samples were measured after 0, 3 and 24 h of incubation at rt. Mass spectra were recorded on a Bruker maXis ESI-Qq-TOF Mass Spectrometer by direct infusion.

*NMR.* Stock solutions in DMF-d$_7$ were prepared and diluted with D$_2$O to achieve a final concentration of 1 mM (10% DMF-d$_7$ content). The complex solution was subjected to incubation

with an equimolar amount of protected amino acids Ac-Cys-OMe, Ac-His-OMe and Ac-Met-OMe, each individually and with a balanced mixture (1 : 1 : 1).

**Oligonucleotide and 9-ethylguanine mass interaction studies**

*9-Ethylguanine.* DMF stock solutions of metal complexes were prepared, mixed with a stock solution of 9-ethylguanine in $H_2O$ and diluted with $H_2O$ to achieve a final concentration of 0.2 mM complex and 0.6 mM 9-ethylguanine (4% DMF content). After 2 h of stirring, the samples were analyzed *via* mass spectrometry. Mass spectra were recorded on an Agilent 6540 QTOF LC/MS Mass Spectrometer by direct infusion.

*Oligonucleotide.* Oligonucleotide was dissolved in 100 mM $NH_4OAc$ solution, heated up to 95 °C for 5 min and cooled down to room temperature slowly. Complex stock solutions in DMF were prepared and diluted with 100 mM $NH_4OAc$ solution to a final concentration of 30 μM. The compound solution was subjected to incubation with equimolar amounts of the oligonucleotide solution (30 μM each) for 2 h under constant stirring before a mass spectrum was recorded. Mass spectra were recorded on an Agilent 6540 QTOF LC/MS Mass Spectrometer by direct infusion.

**$cLog P$ calculation.** The octanol–water partition coefficient $Log P$ was calculated for the free ligands with molinspiration (v2014.11). $cLog P$ values allow the comparison of relative lipophilicities within a series of osmium(II)- or ruthenium(II)-arene metalacycles, as the metal-arene fragments remain unchanged.

**Cell culture.** CH1/PA-1 ovarian teratocarcinoma cells (provided by L. R. Kelland, CRC Centre for Cancer Therapeutics, Institute of Cancer Research, Sutton, UK; confirmed by STR profiling as PA-1 ovarian teratocarcinoma cells at Multiplexion, Heidelberg, Germany), SW480 colon carcinoma and A549 lung adenocarcinoma cells (both obtained from the American Type Culture Collection, Manassas, VA, USA) were grown as adherent cultures in 75 $cm^2$ culture flasks (Starlab, Hamburg, Germany) by using minimal essential medium (MEM) supplemented with 1 mM sodium pyruvate, 4 mM L-glutamine, 1% (v/v) nonessential amino acids from 100-fold stock (all purchased from Sigma-Aldrich) and 10% heat-inactivated fetal bovine serum (BioWest, Nuaillé, France). Cells were maintained under standard culture conditions with 5% $CO_2$ at 37 °C in a humidified atmosphere.

**MTT assay.** The 3-(4,5-dimethylthiazol-2-yl)-2,5-diphenyl-2*H* tetrazolium bromide (MTT, Acros Organics, Geel, Belgium) assay was used to detect the cytotoxicity of the compounds after 96 h incubation. For this purpose, cells were harvested from culture flasks by trypsinization, seeded in 100 μL aliquots into 96-well microculture plates (Starlab, UK) in densities of 1 × $10^3$ (CH1/PA-1), 2 × $10^3$ (SW480) and 3 × $10^3$ (A549) cells per well, and incubated for 24 h prior to exposure to the test compounds. Stock solutions of test compounds were prepared in DMF, which were then diluted in MEM (not to exceed a final content of 0.5% v/v of organic solvent in the test plates), and serial dilutions were added in aliquots of 100 μL per well. After continuous exposure for 96 h, drug solutions were replaced with 100 μL medium/MTT mixtures [6 parts of RPMI

1640 medium supplemented with 10% heat-inactivated fetal bovine serum and 2 mM L-glutamine; 1 part of MTT solution in phosphate buffered saline (5 mg $mL^{-1}$)]. After incubation for 4 h, the medium/MTT mixtures were removed, and the produced formazan crystals were dissolved in 150 μL DMSO per well. Optical densities at 550 nm were measured spectrophotometrically with an ELx808 Absorbance Microplate Reader (Bio-Tek, Winooski, VT, USA) by using a reference wavelength of 690 nm to correct for unspecific absorption. 50% inhibitory concentrations ($IC_{50}$) were interpolated from concentration–effect curves of at least three independent experiments, each comprising triplicates per concentration level.

**Cellular accumulation.** Cellular accumulation of the compounds was studied based on a method described previously[54] with modifications. $1.8 × 10^5$ SW480 cells per well were seeded in aliquots of 1 mL complete MEM (see above) into 12-well plates (CytoOne, tissue culture treated, Starlab, Hamburg, Germany) and incubated at 37 °C for 24 h. Then, cells were exposed for 2 h at 37 °C to 50 μM solutions of the test compounds (containing 0.5% DMF) in fresh 0.5 mL of complete MEM upon exchange of the medium. Afterward, cells were washed three times with 1 mL PBS per well, lysed with 0.4 mL subboiled $HNO_3$ per well for 1 h at room temperature, and 0.3 mL of each sample were diluted with 7.7 mL Milli-Q water. Adsorption/desorption controls were prepared in the same manner in cell-free wells. Ruthenium content was quantified by inductively coupled plasma mass spectrometry (ICPMS) using an ICP-quadrupole MS Agilent 7800 instrument (Agilent Technologies, Waldbronn, Germany) as described previously.[55]

**Cell cycle analysis.** For cell cycle studies SW480 cells were seeded in 12-well plates (CytoOne, tissue culture treated, Starlab) in a density of $6 × 10^4$ cells per well per mL (in MEM). After the recovery time of 24 h, the test compounds (**2c,d**, and **3c,d**) were dissolved in DMF/MEM in a way that the maximum concentration of DMF on the cells did not exceed 0.5%. Plates were incubated at 37 °C, 5% $CO_2$ in a moist atmosphere for 24 h. Gemcitabine (0.05 μM, G1/G0 phase inhibition) and etoposide (0.5 μM, G2/M phase inhibition) were used as positive controls (Fig. S61†). Following the exposure, cells were stained (500 μL per probe) with the DNA-intercalating agent propidium iodide (40 μg $mL^{-1}$; Sigma-Aldrich) diluted in hypotonic fluorochrome solution (HFS: 0.1% (v/v) Triton X-100; 0.1% (w/v) sodium citrate in Milli-Q water). The cells were stained in the dark at 4 °C for 4 h and then collected by vigorous pipetting; diluted with additional 500 μL HFS buffer per probe and left at 4 °C overnight. The fluorescence of all samples stained with propidium iodide was measured 24 h after staining initiation using flow cytometry (Guava easyCyte 8HT, Luminex, Austin, TX, USA). The obtained data sets were evaluated by means of FlowJo software (v. 10.6.1). The cell populations were gated to exclude debris and doublets based on red fluorescence signal intensities (particles width *vs.* height/size). The built-in Watson Pragmatic model was used to analyze the red fluorescence (induced by a green laser: RED-G) intensity histograms. Means and standard deviations were calculated from at least three independently performed experiments.

**Flow cytometric detection of apoptotic/necrotic cells.** For studying apoptosis/necrosis induction by the compounds under investigation, $7 \times 10^4$ SW480 cells per well were seeded in 600 µL per well of complete MEM (see above) into a 24-well plate (CytoOne, tissue culture treated, Starlab) and allowed to re-adhere overnight. After resuming exponential growth, cells were treated with the test compounds in complete MEM (containing $\leq 0.5\%$ v/v DMF) for 24 h and 48 h. The supernatants were collected, adherent cells were washed with 500 µL PBS, and the supernatants collected again. Cells were harvested with trypsin, pooled with the supernatants and centrifuged with $300g$ for 3 min. The supernatant was discarded, 1 µL of annexin V-FITC stock (eBioscience, San Diego, CA, USA) in 150 µL binding buffer (10 mM HEPES/NaOH, pH 7.4, 140 mM NaCl, 2.5 mM $CaCl_2$) were added to the cells, and samples were incubated for 15 min at 37 °C in the dark. Then, 1 µL propidium iodide (PI, 1.0 mg mL$^{-1}$, Sigma-Aldrich) solution in 150 µL binding buffer were added shortly before analysis, and $5 \times 10^3$ events per sample were evaluated with a flow cytometer (Guava easyCyte BGR HT, Luminex, Austin, TX, USA) with guavaSoft 4.5.25. Results are means from at least three independent experiments. The recorded results were analyzed with FlowJo software 10.6.1 (TreeStar, Ashland, OR, USA).

**FRET melting assay.** FRET experiments were conducted on a 96-well format Applied Biosystems™ QuantStudio 6 PCR cycler with a FAM (6-carboxyfluorescein) filter. Stock solutions of oligonucleotides, bearing FAM and TAMRA (6-carboxy-tetramethylrhodamine) probes, were diluted to the desired concentration in 60 mM potassium cacodylate buffer (pH 7.4). c-*MYC* oligonucleotide stock solution was diluted with 10 mM potassium cacodylate since at this buffer concentration its melting temperature was in a reasonable range to observe changes after the interaction with the tested compounds. Subsequently, the oligonucleotides were folded in their B-DNA or G4 topologies by heating the solutions to 95 °C for 5 min, followed by slowly cooling to room temperature overnight. The final concentration of the oligonucleotides was set at 0.2 µM (total volume of 30 µL in each well). Metal complexes were dissolved in DMF to give 2 mM stock solutions and further diluted with the buffer reaching a total percentage of DMF never above 0.3%. Data were collected three times, each time in duplicate, in the range 25–95 °C (with a ramp of 1 °C every 30 s). For comparative analysis across different datasets, emission data were normalized from 0 to 1. $T_{1/2}$ is the temperature at which normalized FAM emission is 0.5.[56] DNA concentration is expressed in strands.

**Circular dichroism.** CD spectra were acquired using a spectropolarimeter Jasco J-715 at 25 °C, incrementally introducing metal complex solution aliquots to a solution of DNA at a constant concentration. The experimental parameters were set as follows: range 400–220 nm, response: 0.5 s, accumulation: 4, speed 200 nm min$^{-1}$. Titrations were performed in Tris-KCl buffer (50 mM Tris-HCl, 100 mM KCl, pH 7.4). Folding of the G4s was obtained as described in the FRET paragraph. DNA concentration is expressed in bases.

**Molecular docking.** The structures of the metal complexes underwent optimization through Density Functional Theory (DFT) calculations within the Gaussian16 program package.[57] The m06l functional[58] was employed, along with the LANL2TZ (f) pseudopotential basis set for metal atoms[59] and the 6-311G (d,p) basis set for other atoms.[60] Autodock Tools 1.5.6[61] was used to generate the pdbqt files of c-*KIT1* (PDB id: 2O3M), c-*MYC* (PDB id: 1XAV) and the compounds (**2a**, **2c**, **2d**). Blind docking was achieved generating a grid box large enough to include all the possible binding sites of the G4 structures. In particular, grid box sizes for c-*MYC* were 80 Å × 80 Å × 80 Å, with a grid spacing of 0.375 Å and −0.062, 1.272, 0.974 for central grid point xyz-coordinates. As for c-*KIT1*, grid box sizes were 80 Å × 80 Å × 80 Å, with a grid spacing of 0.375 A° and −1.029, 4.110, −1.269 for central grid point xyz-coordinates. Molecular docking was performed using AutoDock 4.2.[61] Docking was performed using the Lamarckian Genetic Algorithm. Estimated free energies of binding are expressed in kcal mol$^{-1}$. Figures were generated using ChimeraX.[62]

## Conclusions

Within this work, the synthesis of ten 4-phenylthiazole derived ruthena(II)- and osma(II)cycles is described. The obtained complexes were characterized by means of standard analytical techniques and their aqueous stability and interaction with biological molecules were investigated. Amino acid interaction studies showed a stronger affinity towards L-methionine compared to L-histidine and L-cysteine. DNA interaction studies revealed that compounds **2a**, **2c** and **2d** induced a stabilizing effect on G-quadruplex structures with a clear preference of compound **2c** for G4 forming in the promoter of the oncogene c-*myc*. While docking calculations suggested that the *R* enantiomer interacts tighter with the mentioned DNA motif, mass analysis proved the formation of a **2c**-c-*MYC* adduct. Additionally, the IC$_{50}$ values of all metalacycles and the corresponding free ligands were determined in three human cancer cell lines (A549, SW480 and CH1/PA-1). While the ligands show no cytotoxic effect in the tested concentration range, the respective complexes proved to be highly active, with IC$_{50}$ values in the low micromolar range. Except for **2a**, higher cellular accumulation is in alignment with higher cytotoxicity. Surprisingly, no clear correlation between lipophilicity and drug accumulation was found. Selected compounds only exhibit a slow and weak induction of apoptosis and only minor cell cycle perturbations were observed.

## Author contributions

Conceptualization, A. T., B.K. K. and W.K.; data curation, P. G., A. T., O. D., M. A. J. and W. K.; formal analysis, P. G., L. M., E. T., A. P.-R., M. H., K. C., A. A. L., O. D. and G. B.; funding acquisition, O. D., A. T., B. K. K. and W. K.; investigation, P. G., L. M., E. T., O. D., K. C., M. H., A. P.-R., and A. A. L.; method-

ology, G. B., A. T., M. A. J., B. K. K. and W. K.; project administration, A. T., B. K. K. and W. K.; resources, O. D., M. A. J., G. B., A. T., B. K. K. and W. K.; software, G. B.; supervision, M. A. J., A. T., B. K. K. and W. K.; validation, O. D., M. A. J., G. B., A. T., B. K. K. and W. K.; visualization, P. G., O. D., K. C., A. P.-R., A. A. L., M. A. J., A. T., G. B. and W. K.; writing–original draft preparation, P. G., L. M., O. D., A. A. L, M. A. J., A. T. and W. K.; writing–review and editing, P. G., M. A. J., A. T. and W. K.; All authors have read and agreed to the published version of the manuscript.

## Conflicts of interest

There are no conflicts to declare.

## Acknowledgements

## References

1 B. Rosenberg, *New Agents for the Control of Tumours*, 1971, **15**, 42–51.

2 D. Wang and S. J. Lippard, *Nat. Rev. Drug Discovery*, 2005, **4**, 307–320.

3 E. J. Anthony, E. M. Bolitho, H. E. Bridgewater, O. W. L. Carter, J. M. Donnelly, C. Imberti, E. C. Lant, F. Lermyte, R. J. Needham, M. Palau, P. J. Sadler, H. Shi, F. X. Wang, W. Y. Zhang and Z. Zhang, *Chem. Sci.*, 2020, **11**, 12888–12917.

4 R. Oun, Y. E. Moussa and N. J. Wheate, *Dalton Trans.*, 2018, **47**, 6645–6653.

5 M. A. Jakupec, M. S. Galanski, V. B. Arion, C. G. Hartinger and B. K. Keppler, *Dalton Trans.*, 2008, 183–194.

6 J. P. C. Coverdale, T. Laroiya-McCarron and I. Romero-Canelón, *Inorganics*, 2019, **7**, 31.

7 R. Trondl, P. Heffeter, C. R. Kowol, M. A. Jakupec, W. Berger and B. K. Keppler, *Chem. Sci.*, 2014, **5**, 2925–2932.

8 L. S. Flocke, R. Trondl, M. A. Jakupec and B. K. Keppler, *Investig. New Drugs.*, 2016, **34**, 261–268.

9 C. Chen, C. Xu, T. Li, S. Lu, F. Luo and H. Wang, *Eur. J. Med. Chem.*, 2020, **203**, 112605.

10 G. M. O'Kane, J. L. Spratlin, D.-Y. Oh, S. Y. Rha, E. Elimova, P. Kavan, M. K. Choi, R. A. Goodwin, S. T. Kim, D.-H. Koo, K. Halani, E. R. McAllister, M. Jones, M. Snow, Y. Lemmerick, G. Spera and J. Pankovich, *J. Clin. Oncol.*, 2023, **41**, 4098.

11 M. A. Jakupec, E. Reisner, A. Eichinger, M. Pongratz, V. B. Arion, M. Galanski, C. G. Hartinger and B. K. Keppler, *J. Med. Chem.*, 2005, **48**, 2831–2837.

12 J. Karges, *Angew. Chem., Int. Ed.*, 2022, **61**, e202112236.

13 G. S. Kulkarni, K. A. Richards, P. C. Black, R. A. Rendon, J. Chin, N. D. Shore, G. Jayram, E. V. Kramolowsky, D. Saltzstein, P. K. Agarwal, L. Belkoff, M. A. O'Donnell, A. M. Kamat, M. A. S. Jewett, D. L. Lamm, V. DeGruttola, A. Mandel, R. Dumoulin-White and W. Kassouf, *J. Clin. Oncol.*, 2023, **41**, 528.

14 A. Chettri, T. Yang, H. D. Cole, G. Shi, C. G. Cameron, S. A. McFarland and B. Dietzek-Ivanšić, *Angew. Chem., Int. Ed.*, 2023, **62**, e202301452.

15 C. A. Riedl, L. S. Flocke, M. Hejl, A. Roller, M. H. M. Klose, M. A. Jakupec, W. Kandioller and B. K. Keppler, *Inorg. Chem.*, 2017, **56**, 528–541.

16 W. D. J. Tremlett, D. M. Goodman, T. R. Steel, S. Kumar, A. Wieczorek-Błauż, F. P. Walsh, M. P. Sullivan, M. Hanif and C. G. Hartinger, *Coord. Chem. Rev.*, 2021, **445**, 213950.

17 C. A. Riedl, M. Hejl, M. H. M. Klose, A. Roller, M. A. Jakupec, W. Kandioller and B. K. Keppler, *Dalton Trans.*, 2018, **47**, 4625–4638.

18 A. Bergamo, C. Gaiddon, J. H. M. Schellens, J. H. Beijnen and G. Sava, *J. Inorg. Biochem.*, 2012, **106**, 90–99.

19 R. E. Aird, J. Cummings, A. A. Ritchie, M. Muir, R. E. Morris, H. Chen, P. J. Sadler and D. I. Jodrell, *Br. J. Cancer*, 2002, **86**, 1652–1657.

20 W. H. Ang, A. Casini, G. Sava and P. J. Dyson, *J. Organomet. Chem.*, 2011, **696**, 989–998.

21 B. S. Murray, M. V. Babak, C. G. Hartinger and P. J. Dyson, *Coord. Chem. Rev.*, 2016, **306**, 86–114.

22 F. Wang, A. Habtemariam, E. P. L. van der Geer, R. Fernández, M. Melchart, R. J. Deeth, R. Aird, S. Guichard, F. P. A. Fabbiani, P. Lozano-Casal, I. D. H. Oswald, D. I. Jodrell, S. Parsons and P. J. Sadler, *Proc. Natl. Acad. Sci. U. S. A.*, 2005, **102**, 18269–18274.

23 A. F. A. Peacock, M. Melchart, R. J. Deeth, A. Habtemariam, S. Parsons and P. J. Sadler, *Chem. – Eur. J.*, 2007, **13**, 2601–2613.

24 M. Schmidlehner, V. Pichler, A. Roller, M. A. Jakupec, W. Kandioller and B. K. Keppler, *J. Organomet. Chem.*, 2015, **782**, 69–76.

25 S. Mokesch, K. Cseh, H. Geisler, M. Hejl, M. H. M. Klose, A. Roller, S. M. Meier-Menches, M. A. Jakupec, W. Kandioller and B. K. Keppler, *Front. Chem.*, 2020, **8**, 1–15.

26 M. Martínez-Alonso, N. Busto, F. A. Jalón, B. R. Manzano, J. M. Leal, A. M. Rodríguez, B. García and G. Espino, *Inorg. Chem.*, 2014, **53**, 11274–11288.

27 L. Belsa, C. López, A. González, M. Font-Bardía, T. Calvet, C. Calvis and R. Messeguer, *Organometallics*, 2013, **32**, 7264–7267.

28 J. Ruiz, V. Rodríguez, N. Cutillas, A. Espinosa and M. J. Hannon, *Inorg. Chem.*, 2011, **50**, 9164–9171.

29 G. S. Yellol, A. Donaire, J. G. Yellol, V. Vasylyeva, C. Janiak and J. Ruiz, *Chem. Commun.*, 2013, **49**, 11533–11535.

30 J. Yellol, S. A. Pérez, A. Buceta, G. Yellol, A. Donaire, P. Szumlas, P. J. Bednarski, G. Makhloufi, C. Janiak, A. Espinosa and J. Ruiz, *J. Med. Chem.*, 2015, **58**, 7310–7327.

31 B. Boff, C. Gaiddon and M. Pfeffer, *Inorg. Chem.*, 2013, **52**, 2705–2715.

32 W. Lee, C. Shin, S. E. Park and J. M. Joo, *J. Org. Chem.*, 2019, **84**, 12913–12924.

33 E. Ferrer Flegeau, C. Bruneau, P. H. Dixneuf and A. Jutand, *J. Am. Chem. Soc.*, 2011, **133**, 10161–10170.

34 A. F. A. Peacock, A. Habtemariam, R. Fernández, V. Walland, F. P. A. Fabbiani, S. Parsons, R. E. Aird, D. I. Jodrell and P. J. Sadler, *J. Am. Chem. Soc.*, 2006, **128**, 1739–1748.

35 S. Mokesch, M. S. Novak, A. Roller, M. A. Jakupec, W. Kandioller and B. K. Keppler, *Organometallics*, 2015, **34**, 848–857.

36 W. Kandioller, C. G. Hartinger, A. A. Nazarov, C. Bartel, M. Skocic, M. A. Jakupec, V. B. Arion and B. K. Keppler, *Chem. – Eur. J.*, 2009, **15**, 12283–12291.

37 A. C. Komor and J. K. Barton, *Chem. Commun.*, 2013, **49**, 3617–3630.

38 J. Qian, R. Liu, N. Liu, C. Yuan, Q. Wu, Y. Chen, W. Tan and W. Mei, *Molecules*, 2022, **27**, 3046.

39 Q. Wu, K. Zheng, S. Liao, Y. Ding, Y. Li and W. Mei, *Organometallics*, 2016, **35**, 317–326.

40 W. Streciwilk, A. Terenzi, R. Misgeld, C. Frias, P. G. Jones, A. Prokop, B. K. Keppler and I. Ott, *ChemMedChem*, 2017, **12**, 214–225.

41 W. Streciwilk, A. Terenzi, F. Lo Nardo, P. Prochnow, J. E. Bandow, B. K. Keppler and I. Ott, *Eur. J. Inorg. Chem.*, 2018, **2018**, 3104–3112.

42 L. A. Hager, S. Mokesch, C. Kieler, S. Alonso-de Castro, D. Baier, A. Roller, W. Kandioller, B. K. Keppler, W. Berger, L. Salassa and A. Terenzi, *Dalton Trans.*, 2019, **48**, 12040–12049.

43 D. Varshney, J. Spiegel, K. Zyner, D. Tannahill and S. Balasubramanian, *Nat. Rev. Mol. Cell Biol.*, 2020, **21**, 459–474.

44 G. W. Collie, G. N. Parkinson, S. Neidle, F. Rosu, E. De Pauw and V. Gabelica, *J. Am. Chem. Soc.*, 2010, **132**, 9328–9334.

45 T. Kench and R. Vilar, in *Annual Reports in Medicinal Chemistry*, Academic Press Inc., 2020, vol. 54, pp. 485–515.

46 H. Geisler, S. Harringer, D. Wenisch, R. Urban, M. A. Jakupec, W. Kandioller and B. K. Keppler, *ChemistryOpen*, 2022, **11**, e202200019.

47 S. Tani, T. N. Uehara, J. Yamaguchi and K. Itami, *Chem. Sci.*, 2014, **5**, 123–135.

48 G. M. Sheldrick, *Acta Crystallogr., Sect. A: Found. Adv.*, 2015, **71**, 3–8.

49 G. M. Sheldrick, *Acta Crystallogr., Sect. C: Struct. Chem.*, 2015, **71**, 3–8.

50 O. V. Dolomanov, L. J. Bourhis, R. J. Gildea, J. A. K. Howard and H. Puschmann, *J. Appl. Crystallogr.*, 2009, **42**, 339–341.

51 C. B. Hübschle, G. M. Sheldrick and B. Dittrich, *J. Appl. Crystallogr.*, 2011, **44**, 1281–1284.

52 O. Dömötör, S. Aicher, M. Schmidlehner, M. S. Novak, A. Roller, M. A. Jakupec, W. Kandioller, C. G. Hartinger, B. K. Keppler and É. A. Enyedy, *J. Inorg. Biochem.*, 2014, **134**, 57–65.

53 P. Gans, A. Sabatini and A. Vacca, *Talanta*, 1996, **43**, 1739–1753.

54 A. E. Egger, C. Rappel, M. A. Jakupec, C. G. Hartinger, P. Heffeter and B. K. Keppler, *J. Anal. At. Spectrom.*, 2009, **24**, 51–61.

55 K. Cseh, H. Geisler, K. Stanojkovska, J. Westermayr, P. Brunmayr, D. Wenisch, N. Gajic, M. Hejl, M. Schaier, G. Koellensperger, M. A. Jakupec, P. Marquetand and W. Kandioller, *Pharmaceutics*, 2022, **14**, 2644.

56 L. D'Anna, S. Rubino, C. Pipitone, G. Serio, C. Gentile, A. Palumbo Piccionello, F. Giannici, G. Barone and A. Terenzi, *Dalton Trans.*, 2022, **52**, 2966–2975.

57 M. J. Frisch, G. W. Trucks, H. B. Schlegel, G. E. Scuseria, M. A. Robb, J. R. Cheeseman, G. Scalmani, V. Barone, G. A. Petersson, H. Nakatsuji, X. Li, M. Caricato, A. V. Marenich, J. Bloino, B. G. Janesko, R. Gomperts, B. Mennucci, H. P. Hratchian, J. V. Ortiz, A. F. Izmaylov, J. L. Sonnenberg, D. Williams-Young, F. Ding, F. Lipparini, F. Egidi, J. Goings, B. Peng, A. Petrone, T. Henderson, D. Ranasinghe, V. G. Zakrzewski, J. Gao, N. Rega, G. Zheng, W. Liang, M. Hada, M. Ehara, K. Toyota, R. Fukuda, J. Hasegawa, M. Ishida, T. Nakajima, Y. Honda, O. Kitao, H. Nakai, T. Vreven, K. Throssell, J. A. Montgomery Jr., J. E. Peralta, F. Ogliaro, M. J. Bearpark, J. J. Heyd, E. N. Brothers, K. N. Kudin, V. N. Staroverov, T. A. Keith, R. Kobayashi, J. Normand, K. Raghavachari, A. P. Rendell, J. C. Burant, S. S. Iyengar, J. Tomasi, M. Cossi, J. M. Millam, M. Klene, C. Adamo, R. Cammi, J. W. Ochterski, R. L. Martin, K. Morokuma, O. Farkas, J. B. Foresman and D. J. Fox, Gaussian, Inc, Wallingford CT, 2016.

58 Y. Wang, X. Jin, H. S. Yu, D. G. Truhlar and X. He, *Proc. Natl. Acad. Sci. U. S. A.*, 2017, **114**, 8487–8492.

59 A. W. Ehlers, M. Böhme, S. Dapprich, A. Gobbi, A. Höllwarth, V. Jonas, K. F. Köhler, R. Stegmann, A. Veldkamp and G. Frenking, *Chem. Phys. Lett.*, 1993, **208**, 111–114.

60 R. Krishnan, J. S. Binkley, R. Seeger and J. A. Pople, *J. Chem. Phys.*, 2008, **72**, 650–654.

61 G. M. Morris, H. Ruth, W. Lindstrom, M. F. Sanner, R. K. Belew, D. S. Goodsell and A. J. Olson, *J. Comput. Chem.*, 2009, **30**, 2785–2791.

62 E. F. Pettersen, T. D. Goddard, C. C. Huang, E. C. Meng, G. S. Couch, T. I. Croll, J. H. Morris and T. E. Ferrin, *Protein Sci.*, 2021, **30**, 70–82.